Intra-arc Crustal Seismicity: Seismo-tectonic Implications for the Southern Andes Volcanic Zone, Chile

Gerd Sielfeld[1,2], Dietrich Lange[3], and José Cembrano[1,2]

[1]Pontificia Universidad Católica de Chile, Chile.

[2]Centro de Excelencia en Geotermia de Los Andes, CEGA, Chile.

[3]GEOMAR Helmholtz Centre for Ocean Research Kiel, Germany.

Corresponding author: Gerd Sielfeld (ggsielfeld@uc.cl)

†alternative email gsielfeld@gmail.com

Key Points:

- Crustal seismicity in the SVZ of the Andes reveals the nature of active upper crustal faulting consistent with long-term arc tectonics

- Strain partitioning is compartmentalized into arc-parallel (LOFS) and Andean transverse faults (ATF)

  Crustal seismicity occurs at all depths down to 40 km depth in the forearc, but shallower than 12 km along the volcanic chain

Abstract

We examine the intra-arc crustal seismicity of the Southern Andes Volcanic Zone (SVZ). Our aim is to resolve inter-seismic deformation in an active magmatic arc dominated by both margin-parallel (Liquiñe-Ofqui fault system, (LOFS)) and Andean transverse faults (ATF). Crustal seismicity provides information about the schizosphere tectonic state, delineating the geometry and kinematics of high strain domains driven by oblique-subduction. Here, we present local seismicity based on 16-months data collected from 34 seismometers monitoring a ~200 km long section of the Southern Volcanic Zone, including the Lonquimay and Villarrica volcanoes. We located 356 crustal events with magnitudes between M_w 0.6 and M_w 3.6. Local seismicity occurs at depths down to 40 km in the forearc and consistently shallower than 12 km beneath the volcanic chain, suggesting a convex shape of the crustal seismogenic layer bottom. Focal mechanisms indicate strike-slip faulting consistent with ENE-WSW shortening in line with the long-term deformation history revealed by structural geology studies. However, we find regional to local-scale variations in the shortening axes orientation as revealed by the nature and spatial distribution of microseismicity, within three distinctive latitudinal domains. In the northernmost domain, seismicity is consistent with splay faulting at the northern termination of the LOFS; in the central domain, seismicity distributes along ENE- and WNW-striking discrete faults, spatially associated with, hitherto seismic ATF. The southernmost domain, in turn, is characterized by activity focused along a N15°E striking master branch of the LOFS. These observations indicate a complex strain compartmentalization pattern within the intra-arc crust, where variable strike-slip faulting dominates over dip-slip movements.

Plain Language Summary

In active volcanic chains, there is a strong interplay between deformation and volcanism. In this research, we take the "pulse" of active tectonics in a volcanic arc setting by measuring natural seismicity. We installed a network of 34 seismometers over 200 km along the volcanic arc in Southcentral Chile. Our results indicate active faulting in coherence with long-lived faults and the overall regional-scale stress regime. In fact, crustal regions in which faults are more active, are spatially associated with inherited faults and with higher temperature gradient domains, as inferred from volcanic and geothermal activity. The maximum depth of seismicity is shallow (<12 km) in the central part of the volcanic arc, whereas is much deeper (~40 km) towards the forearc and back-arc regions. This observation suggests that elevated geothermal gradients lead to a thinner brittle portion of crust, which is then mechanically easier to (re-)break up. Our results can be used for understanding the way by which faulting interacts with crustal fluids, which in turn may help improving geothermal exploration strategies and seismic hazard assessment. Furthermore, seismicity reveals detailed information on how ongoing deformation accommodates within complex fault systems characterized by different orientations and kinematics.

1 Introduction

Crustal faulting is an end-member effect of large scale tectonic loading. At active magmatic arcs in an oblique convergence setting, permanent heat flow enhances margin-parallel rock weakening and consequential transpressional partitioning (Tikoff and Teyssier, 1994; De Saint Blanquat et al., 1998). Upper crust seismic faulting represents a snap-shot of instantaneous strain, regarded as stick-slip frictional instability of pre-existing faults (Scholz, 1998). This mechanism refers to sudden "slippage" (earthquake) after an interseismic period of elastic strain accumulation or "stick" (Brace and Byerlee, 1966; Byerlee and Brace, 1968), commonly occurring below the critical temperature of Quartz plasticity (~300˚C; Stesky, 1975). Furthermore, crustal earthquakes within magmatic arcs are either purely tectonic, spatially associated with major intra-arc strike-slip faults (e.g. Weller et al., 2012; White, 1991; White and Harlow, 1993; La Femina et al., 2002) or have a volcanic component, associated with magma flux, degassing and volcanic processes (e.g. Manga and Brodsky, 2006; Jay et al., 2011; Patanè et al., 2011; Mora-Stock et al, 2012). Therefore, intra-arc seismicity may reflect the geometry and kinematics of faults and delimit the crustal seismogenic zone, contributing to the understanding of the tectonic and thermo-mechanical state of orogenic belts with active magmatism.

In most subduction settings, long-term oblique convergence slip vectors are partitioned into margin-parallel and margin-orthogonal components (e.g. McCaffrey, 1992). A significant portion of bulk transpressional deformation is commonly accommodated in intra-arc regions, as margin-parallel shear zones (e.g. Fitch, 1972; Beck, 1983; Kimura, 1986; Jarrard, 1986; Beck, 1991; McCaffrey, 1996). In the upper fractured intra-arc crust, deformation is accommodated as strike-slip fault systems for about 50% of active oblique convergence settings (*e.g.* Jarrard, 1986; White, 1991; Bommer et al., 2002). Resulting high strain domains are time-dependent of the interplay among inherited geological anisotropies, fault growth and frictional wear of country rock (Scholz, 1987; Cowie and Scholz, 1992; Joussineau and Aydin, 2009; Mitchell and Faulkner, 2009).

Simultaneously, crustal fluid ascent, differentiation, emplacement and crystallization mechanisms are largely controlled by the geometry, permeability and kinematics of high strain domains (Clemens and Petford, 1999; Cox, 1999; Rowland and Sibson, 2004; Cembrano and Lara, 2009; Acocella and Funiciello, 2010; Yamaguchi, et al., 2011), such as demonstrated for the Sunda, Central-American and Andean magmatic arcs (Sieh and Natawidjaja, 2000; La Femina et al., 2002; Corti et al., 2005; Sielfeld et al., 2017; Iturrieta et al., 2017). Driven by the crustal stress-field and thermal state, fluid migration within such regions (e.g. Nakamura, 1977; Delaney et al.,1986) may be enhanced by rock-dilatancy/fluid-transport mechanisms triggered by shallow seismicity (e.g. Sibson et al., 1975; Scholz, 2002; Rowland and Sibson, 2004).

In the Southern Andes Volcanic Zone (SVZ), in particular along the margin-parallel Liquiñe-Ofqui Fault System (LOFS), stratovolcanoes, minor eruptive centers and geothermal features, are spatially related to the geometry and kinematics of long-lived faults (Cembrano and Lara, 2009; Sánchez-Alfaro et al., 2013). Additionally, for the long-term geological record, margin-parallel faults (*i.e.* LOFS) coexist with second order transverse-to-the-arc oriented faults (Andean Transverse Faults, ATF; Kaizuka, 1968; Katz; 1971; Yañez et al., 1998; Melnick et al., 2009; Aron et al., 2014; among others), developing a causal relationship with crustal fluid-flow (Cembrano and Lara, 2009; Sánchez-Alfaro et al., 2013; Tardani et al., 2016; Wrage, et al., 2017; Pérez-Flores et al., 2016; Pérez-Flores et al, 2017). Based on kinematic and dynamic analysis of fault-slip data, Pérez-Flores et al. (2016) suggest that bulk transpressional deformation is partially partitioned into variable orientations and scales within the Southern Volcanic Zone (SVZ) of the Andean magmatic arc.

Although the present-day instantaneous crustal stress state and slip partitioning effect in the SVZ remains obscure, no dense, regional-scale seismic study has been carried out in the SVZ; consequently, only local deployments associated with specific, moderate to large magnitude events, focussed on the forearc region, have been undertaken in the LOFS. (*e.g.* Lange et al., 2008; Legrand et al. 2010; Dzierma et al., 2012a,b). In this work, we seek to understand the interaction between crustal faulting, strain partitioning and compartmentalization in the upper crust of the intra-arc region of Southern Andes. This will shed light on how a fraction of plate boundary deformation is accommodated in the intra-arc region, during one interseismic-stage of the subduction earthquake cycle. Therefore, we installed a dense seismic network of 34 stations between Callaqui (38˚S) and Mocho-Choshuenco (~40˚S) volcanoes in southern Chile in order to obtain a high-resolution seismicity catalog occurring within an observation time-window of ~16 months (*i.e.* between March 6th 2014 and June 16th 2015).

The study region lies in a transitional zone influenced by two overlapping tectonic loading conditions, associated with two, apparently independent, megathrust seismic cycles. As stated by Sánchez and Drewes (2016), regarding the 2010 Maule M_w 8.8 earthquake post-seismic effects, the region encompassed between 37˚S and 40˚S would have undergone compressional surface deformation from March 2010 to April 2015, with the maximum horizontal stress trending N30˚E (period of GNSS measurements). Conversely, the region south of 38°S has been undergoing interseismic re-loading related to the locking of the 1960 Valdivia M_w 9.5 earthquake rupture zone (Moreno et al., 2009; Moreno et al., 2011). The main target of this experiment is to resolve, for a brief tectonic-time window, the nature and interaction of seismic faulting within (1) long-lived margin-parallel strike-slip fault systems (*i.e* Liquiñe-Ofqui Fault System, LOFS), and (2) long-lived orogeny-oblique faults (Andean-transverse-fault, ATF). Our results contribute to understand the overall link among intra-arc strain compartmentalization, long-lived fault geometries and seismically-active fault kinematics in the framework of an active (Quaternary) volcanic arc.

2 Tectonic setting of Southern Andes

The Southern Andes are characterized by long-term partial partitioning of an overall transpressional deformation regime arising during interseismic phases of the subduction earthquake cycle (e.g. Cembrano et al., 1996; Arancibia et al., 1999; Lavenu and Cembrano, 1999; Pérez-Flores et al., 2016). Dextral-oblique convergence between the Nazca and South American plates trends N80˚, with an average velocity of ca. 66 mm/yr., and mean obliquity of 20° (current convergence vector estimated by Angermann et al., 1999; Fig.1). The convergence vector direction has been relatively constant over the last 10 Ma (Pardo-Casas and Molnar, 1987). Late Miocene- Pliocene transpressional deformation is well documented by field structural geology combined with geochronological data (Arancibia et al., 1999; Lavenu and Cembrano, 1999; Cembrano et al., 2000; Cembrano et al., 2002; Rosenau et al., 2006; Pérez-Flores et al., 2016), as well as by geodetic and seismological studies (e.g. Wang et al., 2007; Moreno et al., 2008, Lange et al., 2008; Haberland et al., 2009; Legrand et al., 2010; Agurto, et al. 2012).

The study area has been affected by two interplate megathrust earthquakes in the last 60 years. The 22 May 1960 Valdivia Mw 9.5 earthquake ruptured > 900 km of the Nazca – South American plates interphase, from Arauco Peninsula (37.5˚) to the Taitao (46.5˚S; Moreno et al., 2009). It is the largest instrumentally recorded seismic event (Engdahl and Villaseñor, 2002). The epicenter took place beneath the Arauco Peninsula, spatially related with forearc strike slip crustal faulting (Lanalhue fault System, LFZ) that has been documented in the past decade (Moreno et al., 2009; Haberland et al., 2006; Fig.1). In turn, the 2010 Maule Mw 8.8 earthquake broke a ~500 km-long portion of the subduction

interphase, extending from 38.2˚S to 34˚S (Moreno et al., 2012). The epicenter locates tens of kilometers north from the Arauco Peninsula (Fig.1), however the coseismic slip is distributed in two main patches, reaching a maximum slip in the northern part of 15.7 m (from GPS measurements; Moreno et al., 2012). Both epicenters locate ~200 km and ~300 km to the WNW and NW of the center of our study area, respectively.

2.1 Liquiñe-Ofqui Fault System (LOFS) and Andean-transverse Faults (ATF)

The LOFS is a 1200 km-long intra-arc dextral strike-slip structure, characterized by master NNE-striking dextral strike-slip fault segments and subsidiary synthetic NE- to ENE-striking transtensional faults (Cembrano and Hervé, 1993; Cembrano et al., 1996, 2000; Melnick et al., 2006a,b). Regional to local-scale transtensional domains, such as duplexes, releasing bends and horsetail geometries have been described (Potent, 2003; Rosenau et al., 2006; Pérez-Flores et al., 2016; Fig. 1) and evidenced by local transtensional seismic faulting (Legrand et al., 2010). In spatial association with these domains, sub-parallel diking, ENE-striking volcanism and hydrothermal activity is a common feature (Melnick et al., 2006a; Rosenau et al., 2006; Lara et al., 2008; Cembrano and Lara, 2009; Sielfeld et al., 2017). Furthermore, tensional stress magnitudes can be larger where NE-striking faults are close to, or intersect, master fault segments, which enhances long-term crustal fluid pathways during interseismic tectonic loading conditions (Iturrieta et al., 2017). A significant portion of the bulk transpressional deformation is accommodated by slip on the intra-arc Liquiñe–Ofqui Fault System (LOFS) displaying markedly slip-rates differences from north to south along different fault segments (Rosenau et al., 2006; Stanton-Yonge et al., 2016; Iturrieta et al, 2017). Calculated slip magnitudes from numerical models may be larger along pure strike-slip fault segments, ranging from ~18 mm/yr., close to southern LOFS termination (Iturrieta et al., 2017), down to 0.5 mm/yr. in the northern termination (Stanton-Yonge et al., 2016; Fig. 1). Thus, as a result of highly coupled plate interfaces, the forearc sliver motion, and thermal weakness at the intra-arc region (Cembrano et al., 2002; Wang et al., 2007), the overriding plate shows a variable degree of deformation partitioning along and across the Southern Andes (Arancibia et al., 1999; Lavenu and Cembrano, 1999; Rosenau et al., 2006; Pérez-Flores et al., 2016). The LOFS records long-term right-lateral ductile deformation between 6 and 3 Ma (Cembrano et al., 2000) that is overprinted by dextral brittle deformation since 1.6 Ma (Lavenu and Cembrano, 1999). Present-day activity of this fault system is consistent with northward motion (6.5 mm/yr.) of the forearc sliver (Wang et al., 2007) and available crustal seismic faulting (Fig. 1). A compilation of focal mechanisms between -33 and -44˚S shown in Fig. 1, clearly document dextral strike-slip partitioning accommodated in the intra-arc (Chinn and Isacks, 1983; Barrientos and Acevedo-Aranguiz, 1992; Lange et al., 2008; gCMT, http://www.gcmt.org).

Andean transverse faults (ATF) are WNW-striking, long-lived structures recognized as conspicuous morphotectonic lineaments and fault zones striking obliquely with respect to the overall Andean orogeny strike (~N10˚E). ATFs are suggested to be older or coeval to the LOFS (e.g. Pankhrust, et al., 2006; Rivera and Cembrano, 2000; Moreno et al., 2011), and have been suggested to play a first-order role in SW Gondwana Carboniferous-Permian basin evolution and the Carboniferous accretion of the Patagonian terrain (Breitkreuz, 1991; Tankard, et al., 1995, Rapela et al., 2003; Pankhrust et al., 2006). ATFs also have been thought to control the Neogene forearc basin architecture and megathrust rupture segmentation associated with the seismic subduction cycle (Glodny et al., 2008; Melnick et al., 2009). Furthermore, deformation of the ATFs might be activated from megathrust earthquakes (Arriagada et al., 2011; Farías et al., 2011; Aron et al., 2014; Stanton-Yonge et al., 2016), and may control crustal fluid migration within the intra-arc region (Katz, 1971;

Rivera and Cembrano, 2000; Cembrano and Lara, 2009; Sánchez et al., 2013; Sielfeld, et al., 2017; Pérez-Flores et al., 2016; Roquer et al., 2016; Wrage et al., 2017).
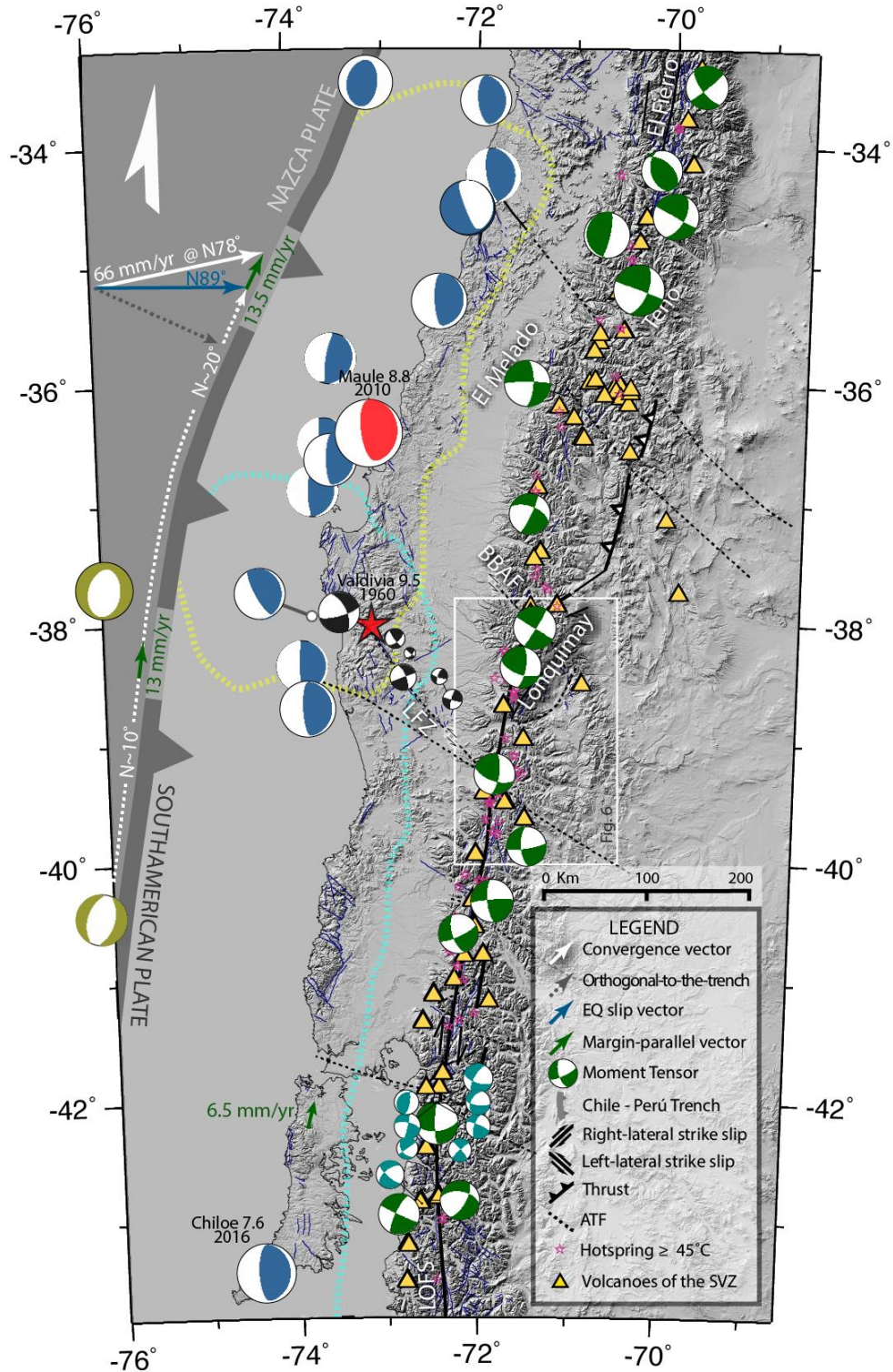

Fig. 1: Seismotectonic map of the southern Andes. Convergence rate and direction is shown by the solid white vector (Angermann et al., 1999). Approximate coseismic rupture zones (slip>1m) of the 1960 Valdivia M_w 9.5 (epicenter in red star) and 2010 Maule (moment tensor in red-white) megathrust earthquakes are outlined by cyan and yellow dashed lines, respectively (Moreno et al., 2009; Moreno et al., 2012). Moment tensors of the gCMT catalog (www.globalcmt.org, 1976-2017) include: i) 13 subduction-type earthquakes (blue-white beach-

balls M_w > 6.5) ratifying the average slip accommodated in the subduction interphase; ii) outer-rise seismicity M_w > 6.5 (beige-white beach-balls); iii) crustal events $M_w \geq 5$ and depth < 20 km in green-white beach-balls. Crustal focal mechanisms from local deployments are shown in black-white (Haberland et al., 2006) and light blue-white (Lange et al., 2008). Focal mechanisms are scaled proportional to their moment magnitude (factor 0.4). Location of geothermal springs and stratovolcanoes taken from Hauser, 1997, Risacher and Hauser, 2008 and Siebert et al., 2010. Crustal faults systems (LOFS, ATF) and morphotectonic lineaments from Melnick and Echtler (2006), Cembrano and Lara, 2009, Lira et al., 2015; Pérez-Flores et al., 2016. Margin orthogonal and margin-parallel components are schematized in dashed arrows. Average slip vector of subduction thrust earthquakes are indicated in blue. The expected residual margin-parallel slip component is shown by green vectors (Stanton-Yonge et al., 2016). The rectangle in white lines represent the area shown in Figures 6 and S1. Shaded relief image generated with 1 arc-second (~30 m) resolution data from the Shuttle Radar Topography Mission.

2.2 Nature and historical record of intra-arc seismicity

In general, intra-arc upper crustal seismicity sources are either pure tectonic or related to sub-volcanic and volcanic processes (Zobin, 2003). Tectonic wave forms, in which this paper is focused, are characterized by *P* and *S* body-wave onsets; the largest reported magnitudes are of ~7.5 *(M_w)* associated with the activation of long segments of arc-parallel strike-slip faults such as in Central America or in Sumatra (Reid, 1913; White and Harlow, 1993). Intra-arc volcanic seismicity, in turn, involves a wide spectra of low-frequency (long-period) quakes associated with subsurface to surface magmatic processes, *i.e.* shear and tensile failures within volcanic edifices, fluid pressurization, diking, volume changes, degassing, among others (Zobin, 2003; Chouet, 2003; Manga and Brodsky, 2006). For instance, the biggest recorded volcanic events are ~5.7 M_l (*e.g.* in 1981 Mt. St. Helens eruptive cycle, and 1991 Mt. Pinatubo eruption; Mori et al., 1991). Nonetheless, strong to mega tectonic earthquakes cause small static stress changes in the crust, which may perturb and potentially trigger eruptions at primed volcanoes (*e.g.* Mt Fuji's 1707 eruption, linked to M 8.7 Hoei earthquake at the Nankai megathrust; Chelsey et al., 2012).

Few and sparse local seismic networks in Southern Andes have reported shallow crustal seismicity (depth <20 km) along several domains of the Southern Volcanic Zone (SVZ) (e.g. Barrientos and Acevedo-Aránguiz, 1992; Farías et al, 2010; Mora-Stock et al, 2012; Cardona et al., 2015) and the LOFS (Bohm, et al., 2002; Lange et al., 2008; Legrand et al., 2010; Agurto et al., 2012). Several of the observed events, are of magnitude 5 or greater, including two M_w 6.1 and M_w 6.2 Aysen Fjord earthquakes in April 2007, associated with a strike-slip duplex at the southern termination of the LOFS (e.g. Legrand, et al., 2010; Mora-Stock et al., 2010; Agurto et al., 2012); the strike-slip El Melado 6.0 *(M_w)* earthquake in the Maule region in June 2012 (indicated in Fig. 1), spatially associated with the NS trending El Melado River Lineament (Cardona et al., 2015); and the M_w 6.5 Teno earthquake in August 2004, associated with dextral strike-slip on El Fierro Fault (gCMT; Farías et al., 2010; Fig. 1). At Lonquimay volcano (38°22'S), one 5.3 *(M_w)* earthquake on February 24th (1989) was recorded at 15 km depth two months after a flank cone eruption, (Strombolian "Navidad crater" eruption on December 25th, 1988; Barrientos and Acevedo-Aránguiz, 1992; Fig. 1). Volcano-tectonic events distribution and moment tensor of the M_w 5.3 quake (gCMT; Dziewonski et al., 1990) indicate right lateral strike-slip faulting along the NNE-striking Lolco Fault of the LOFS (Barrientos and Acevedo-Aránguiz, 1992).

In contrast, sparse and small magnitude crustal earthquakes have been recorded along the ATFs. For instance, left-lateral strike-slip to compressive focal mechanisms (Haberland et al., 2006) were reported for the NW-striking Lanalhue Fault Zone in the forearc region of southcentral Chile (LFZ; Fig. 1) (Melnick and Echtler, 2006, Haberland et al., 2006). Further, south in the main Andes (41.5°S - 43.5°S), Lange et al. (2008) observed seismic clusters associated with secondary NW left-lateral strike slip faulting cross-cutting the LOFS close to strato-volcanoes, with focal mechanisms in line with the long-term stress fields estimated

from faults-slip data inversions along the volcanic arc (Lavenu and Cembrano, 1999; Iturrieta et al., 2017).

Similarly, at the northern termination of the LOFS, the strike-slip Callaqui-Alto Biobio earthquake ($M_w = 5.5$) occurred on December 2006, close to a fault intersection. Tele-seismically detected (Fig. 1, NEIC - gCMT), the epicenter is located in between the NW-striking Biobio-Aluminé Fault (BBAF) and the NNE-striking Lolco-Lomin Fault segment of the LOFS (Fig. 1). Hypocenter uncertainty does not allow to correlate this event to either the LOFS or the BBAF. More importantly, all above mentioned events are compatible with overall ENE-trending shortening, and NNW-trending extension axes.

3 Data Processing and Methods

We deployed a passive seismic network of 34 stations between 2014 March and 2015 June (~16 months) (Fig. 3 and Fig. S1). The local network consisted of 8 broad-band (Trilium 120) and 25 Mark L4-3D 1 Hz three-component sensors registering ground motion in continuous mode at a 100 Hz sample rate. All instruments were equipped with EarthDataLoggers (Text S1, Figs. S2 and S3). Horizontal separation among the closest stations varies from 6 to 18 km, covering an area of ca. 200 km by 100 km along the magmatic arc (38˚- 40˚S; Fig. 3.b, Table S1 and Fig. S1). Homogenous and dense station-separation allow detection localization of micro-seismicity for the entire zone. In order to assure constant operation in the high mountainous region, including through wintertime, stations were equipped with 90 W solar panels and 65 Ah deep-cycle battery (Text S1, Figs. S2 and S3). Most stations ran continuously, other than 2 high altitude stations (>2000 m a.s.l) that shut down for approximately 3 weeks after heavy snowfall. To further densify the network, we incorporated continuous vertical seismograms of sixteen permanent broadband stations of the Andes Volcanological Observatory (OVDAS), installed on main stratovolcanoes (Fig. S1 and Table S1).

Crustal seismicity level in the region is very low; in fact, no event at all has been listed in the CSN (Centro Sismológico Nacional de Chile) catalog for that period. Therefore, we manually inspected the vertical records of the complete dataset (16 months) using overlapping windows of nine minutes with the Passcal Quick Look software (PQL). Then, *P*- and *S*- waves onsets of local events with *S*-*P*-phase time differences of less than 10 s were manually picked. Overall, the detection and localisation were optimized on the creation of a seismicity catalog down to the smallest possible magnitude events. On average *S*-*P*-phase time difference smaller than 3 s is characteristic for shallow quakes occurring within the study area (see waveform example in Fig. 2). A small number of low and very low period events were detected, but not located; these are then not considered for further analysis. For a total of 652 detected events, *P* and *S* onsets were carefully identified using the software package SEISAN (Ottemöller et al., 2014). For each arrival we manually picked the first possible, the best and last possible arrival times. The error in *P* and *S* determination was then estimated by the differences between the first and last possible arrival time and was then converted into weights. Furthermore, we picked *P*-phase polarities for the stronger events. After phase picking, we used the HYP program, SEISAN modified version of HYPOCENTER location program (Lienert, et al., 1986; Lienert and Havskov, 1995), as a first and linear hypocenter determination approach. The final catalog was selected upon the basis of epicentral distance smaller than 100 km from the network border and hypocentral misfits (RMS, root mean square) smaller then 1 s, from which the 96.9% has RMS smaller than 0.5 [s]. The final catalog consists of 356 crustal events with 2,716 *P*- and 2,323 *S*-phase arrivals. The residual events, not considered here, belong mostly to interplate seismicity.
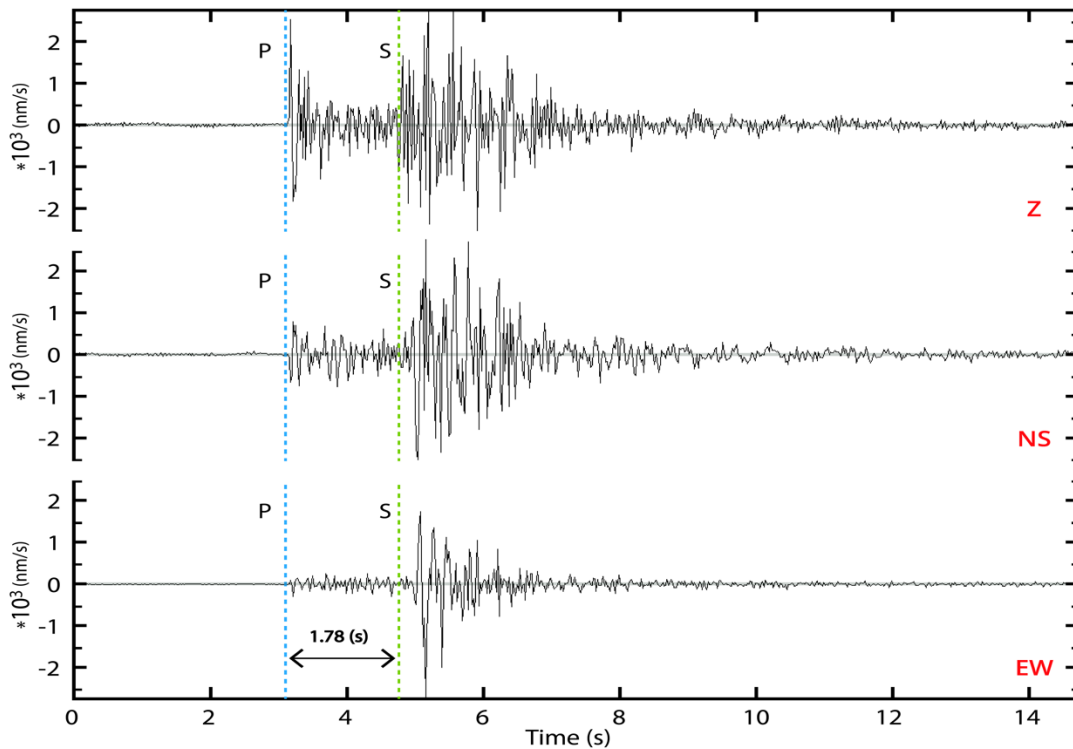
Fig. 2. Raw waveform example of a typical crustal event (8.8 km depth, M_w=1.4 on 18.06.2014, 20:04 UTC) recorded by station LS2S (Fig. 3) at an 11.7 km epicentral distance. Vertical (Z) and horizontal components (NS and EW) are showing impulsive *P* and *S* phase arrivals. A *S-P* time difference of 1.78 [s] indicates a short distance to the source (14.5 km with our velocity model).

3.1 Construction and validation of a minimum one-dimensional (1-d) velocity model

Travel times were used to compute 1-D layered velocity models using VELEST program (Kissling et al., 1995). VELEST inverts 1-D velocity models from phase arrival times, using an initial start-up model (Kissling, 1988; Kissling et al., 1995). Generated results are 1-D *Vp and Vs* velocity models, station corrections (all delays are $< |0.5|$ s), origin-time and hypocentral coordinates (t_o,x,y,z). The following criteria were used for selecting 95 well-constrained earthquakes as inversion input:

i.) minimum of 8 *P*- and 4 *S*-phase arrivals;
ii.) observations within the network (greatest azimuthal gap (GAP)≤180˚);
iii.) event residuals (RMS) smaller than 0.3 s.

We implemented a brute-force search with a large number of plausible *Vp* input models (124.000) and a constant *Vp/Vs* ratio of 1.78, in order to find the minimum 1-D velocity model with the smallest RMS (*e.g.* Lange et al., 2007, 2012). Then, we followed a staggered approach (Husen et al., 1999) using the best *Vp* model (*i.e.* with the smallest RMS) and 60 initial *Vp/Vs* ratios (inverting each 0.1 steps in the range $1.5 < Vp/Vs < 2.1$) to determine a minimum 1-D *Vs* model. The best 1,000 *P*-, and all (60) *S*-velocity models are plotted in Fig. 3, and compared to the minimum 1D *Vp* and *Vs* known for the entire forearc (Haberland et al., 2006). The minimum 1D *Vp* and *Vp/Vs* models are used to determine the final probabilistic hypocenter origin time, coordinates and uncertainty (Lomax, 2000; http://alomax.free.fr/nlloc/).

Fig. 3. a) Computed 1-D *Vp and Vs* velocity models. Thick lines represent the minimum misfit 1D *Vp and Vs* models. The input range of the *Vp* velocity models is indicated by gray dashed lines. Dashed-green lines indicate the minimum *Vp* and *Vs* velocity model obtained for the forearc in this latitudinal range (Haberland et al., 2006). The right panel shows the *Vp/Vs* ratio. b) Stations distribution and P- and S-wave station corrections corresponding to the minimum 1-D *Vp* and *Vs* models. Station names are labeled. Reference station (*Vp* delay = 0 s) is indicated with a black star (LS4S). Stratovolcanoes are indicated with pink triangles. Villarrica volcano (Vi) is shown as reference for Fig. 5.

3.2 Hypocenter Determination and Moment Magnitudes

For the final hypocenter determination, we re-localized the seismicity with the *NonLinLoc* program (Lomax et al., 2000). The program locates seismicity using a non-linear Oct-tree grid-search approach, based on a probabilistic density function (PDF) for the inverse problem of spatial (*x,y,z*) and origin-time (*t*) hypocenter localization (Tarantola and Valette, 1982; Moser et al., 1992; Wittlinger et al., 1993; for a complete description of the method refer to Text S2). The technic provides comprehensive uncertainty and resolution information. The errors in the observations (phase time picks) and in the forward problem (travel-time calculation) are assumed to be Gaussian. This assumption allows the direct analytic calculation of a maximum likelihood origin-time given the observed arrival times and the calculated travel times between the observing stations and a point in the *xyz* space. Thus the 4D problem of hypocenter location reduces to a 3D search over *x,y,z* space (Lomax et al., 2000). The Gaussian estimators and resulting confidence ellipsoid provide location uncertainties, in case the complete non-linear PDF has a single maximum and has an ellipsoidal form. The maximum likelihood location is chosen as the preferred location. For each event, we estimated the three-dimensional spatial confidence (68%) from 3D ellipsoids fitted to 3D PDF scatter clouds.

Seismic moment *(M₀)* as well as moment magnitude *(Mw)* were estimated for all events with more than 4 amplitude readings (265 events). The SEISAN AUTOMAG routine

(Ottemöller and Havskov 2003; Ottemöller et al., 2014) use spectral analysis for making the attenuation and instrument corrected displacement spectrum. This analysis determines the flat spectral level and corner frequency for each record, from which the events seismic moment is calculated.

3.3 Focal Mechanisms

Focal mechanisms yield information about the faulting style. The initial motion of the *P*-wave depends on whether the ray left the source from a compressional (*i.e.* upward first motion at the receiver), or dilatational quadrant (downward first motion at the receiver), easier observed and picked in the vertical component of the receiver. Local events with high quality record, located inside the network (GAP≤180˚) and with at least 8 *P*-, and 4 *S*-wave onsets, and a maximum location misfit (RMS) of 0.3 s were considered. These events had depths ranging from 4 to 15 km, and, moment magnitudes between 1.5 and 3.4 (Table S2). Selected events were first analyzed with FPFIT program (Reasenberg and Oppenheimer, 1985) which use take-off angles (obtained from maximum likelihood hypocenters) to estimate the azimuth and take-off angles at the hypocenter, and determines, from the *P*-wave first arrival polarities, the double coupled force equilibria of the source. In addition to *P*-wave polarities, *S*- to *P*-amplitude ratios provide constraints to the inversion of the source radiation pattern (Kisslinger, 1980). Vertical maximum *P*- and *S*-wave (Pv and Sv) amplitudes were picked in the vertical channel. For each station, horizontal *S*-wave maximum amplitude (Sh) were also picked in the synthetic rotated transverse-to-the-ray-path channel. Take-off angles, *P*-wave polarities and the Sv/Pv, Sv/Sh and Sh/Pv amplitude ratios were used to compute double couple focal mechanisms using the FOCMEC program (Snoke et al., 1984). Finally, we compared solutions obtained from FPFIT and FOCMEC. We only accepted focal mechanism obtained with the FOCMEC approach, which do not differ significantly from the FPFIT solutions (less than 20˚ of difference in primary and auxiliary fault planes). A total of 36 events remained after the selection criteria.

4 Results

4.1 Nature, Magnitudes and Temporal Distribution of Intra-arc Seismicity

Because of the dense station spacing and long-time deployment, we monitored the volcanic arc crustal (micro-)seismicity on a regional scale with very high resolution, for both detection and hypocentral coordinates. Detection and location quality of the 356 crustal events is homogeneous throughout the study area with a magnitude completeness (M_c) of M_w 1.4. Events range from M_w 0.6 to M_w 3.6. Fig. 4 shows our data fitting the Gutenberg-Richter (G-T) relation for magnitudes equal or bigger than M_c. The estimated *b-value* for our experiment is of 1.11 with a maximum magnitude of 3.6 (M_w) in the forearc at 39 km of depth and 3.4 (M_w) in the intra-arc at 9.4 km of depth.
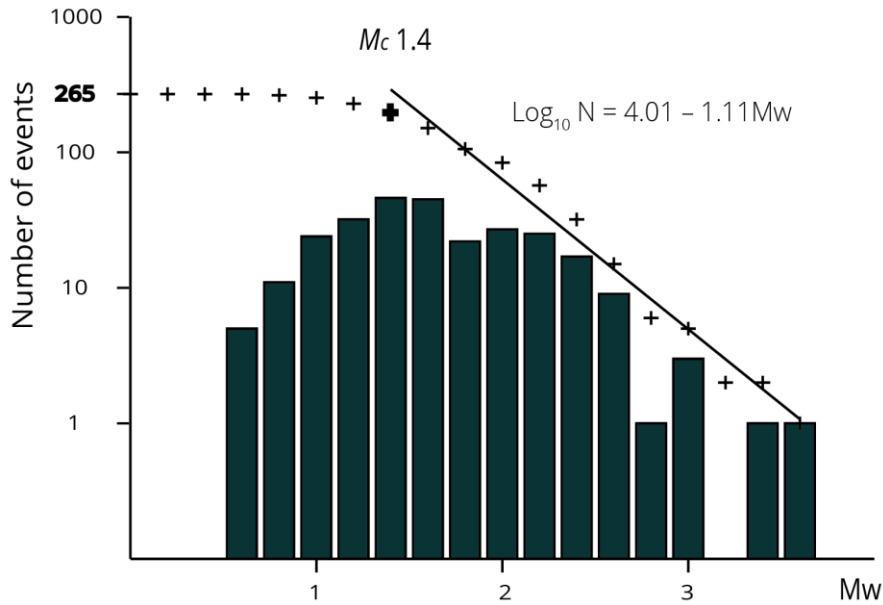
Fig. 4. Magnitude-frequency histogram for the 265 events with calculated magnitudes of our catalog. Columns indicate number of events for each 0.2 units-of-magnitude bin. Crosses represent cumulative number of events per bin. Data fits the Gutenberg-Richter distribution up to the magnitude of completeness (M_{co}), with b-values close to 1.1.

The shallow intra-arc 1-D velocity structure (<9 km) is characterized by relatively low *P*-wave velocities (4.9 km/s in average) compared to *Vp* estimations for the whole forearc from Haberland et al., 2006 (Fig. 3). However below 9 km depth, *P*-wave velocity increases rapidly to 6.2 km/s, demarking a high velocity transition depicted by a seismogenic zone (82% of localized seismicity lies between -1 – 14 km). From that depth down to 35 km, a steadily velocity increment up to 7.3 km/s is estimated. At 40 km depth *Vp* reach 8.3 km/s and *Vp/Vs* drops from 1.82 to 1.59, demarking another first-order velocity discontinuity. Deeper than 40 km velocities are poorly resolved because of limited ray coverage.

Altogether, our ~16-month-long (467 days) experiment recorded 356 crustal events covering an earth surface area of 14,071 km^2. The SAIAS catalog (Southern Andes Intra-Arc Seismicity) is listed in Data Set S1. Activity rate is of 0.762 events per day with an average magnitude of 1.25 *(M_w)*, as is shown in Fig. 5a and 5b. Background level seismicity is characterized by scattered individual events or minor sequences (< 4 events per day) commonly organized in clusters or alignments. Temporal distribution of seismicity (Fig. 5a) depicts five Andean-transverse seismic sequences with more than 5 events per day, which are described later on this section. A total of 293 shallow crustal events are located within the intra-arc region, completing the 82.3% of registered quakes. Our results yield to a total seismic moment of 9.7*10^{14} [Nm] for the 16 months of continuous measurement (Fig. 5.c). This is equivalent to a daily seismic moment of 1.476*10^8 [Nm/km^2] which equals a daily moment magnitude of M_w -0.62 units per square kilometer.
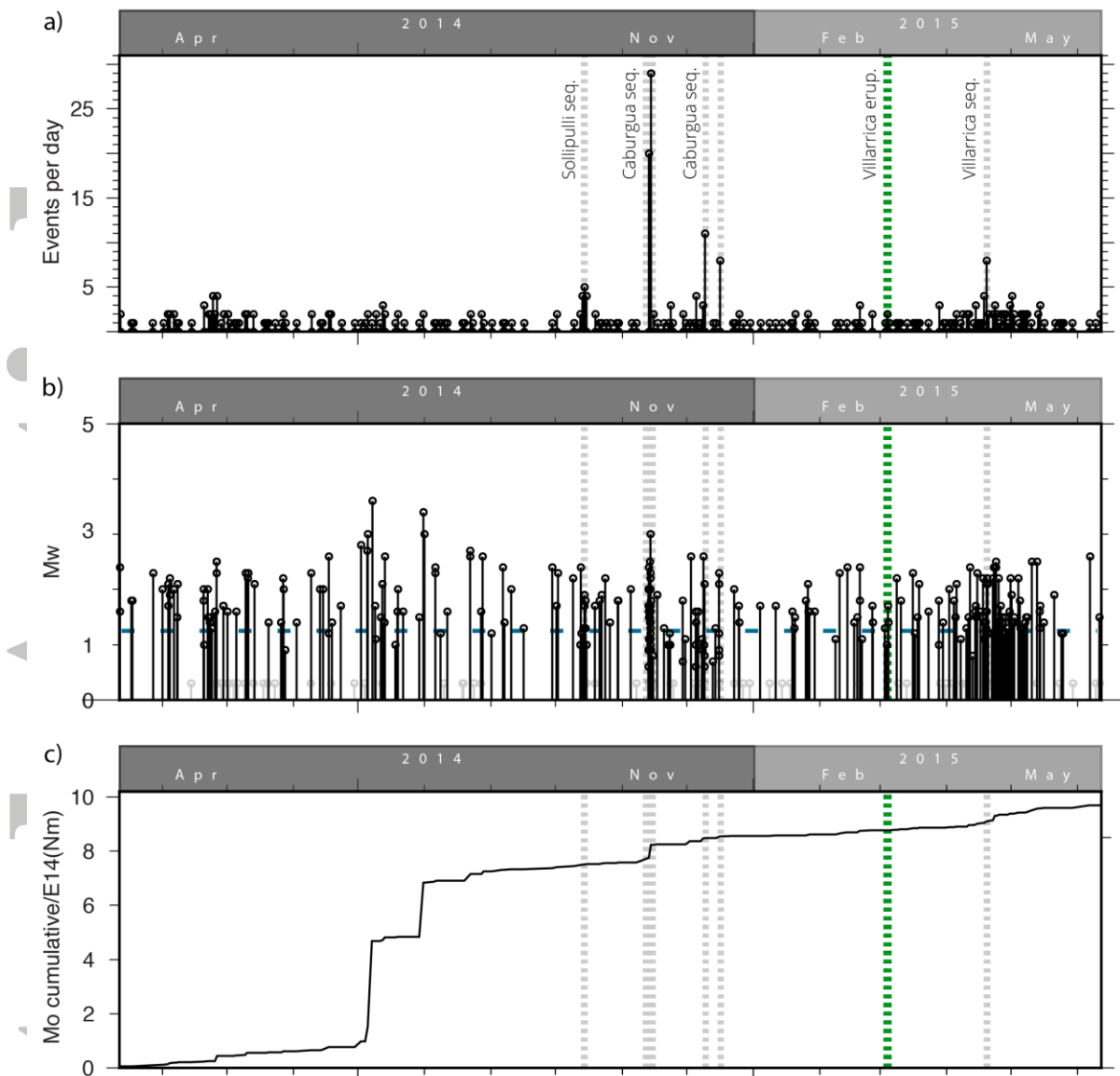
Fig. 5. Temporal properties of the seismicity catalog. a) Number of events per day. b) Total daily moment magnitudes (M_w); Events without magnitude are plotted in gray at 0.3 units. The experiment average M_w is indicated by a dashed blue line. c) Cumulative seismic moment. Green line represents the eruption of Villarrica on 3rd of March 2015. Seismic sequences above the background natural seismicity level are highlighted with gray dashed lines and labelled in panel 'a'.

4.1 Spatial Distribution and Kinematics of Intra-arc Seismicity

Most reported intra-arc events (78.8%) are spatially associated with morphostructural alignments, surface mapped faults and/or ellipsoidal clusters (Fig. 6.a and Video S1). Seismicity follows the overall N10˚E strike of the LOFS and volcanic front and is clustered as NE- or NW striking ellipsoid domains or planes (Fig. 6.a, 6.b and 6.c). The latter, which are hitherto unreported, reveal active deformation in unexpected, and some of them, populated areas. The remaining 21.2% localizes at shallow depth, spatially associated with stratovolcanoes and/or to geothermal features (*e.g.* 62 events occurred within Villarrica volcanic edifice).

Hypocenters beneath the main arc-axis locate between -1 and 16 km. Depths are characterized by a bimodal distribution, defining two levels of relative higher activity: one at 9±2 km and the other at 1±1 km of depth (see histogram in Fig. 6.d). Within these depth

ranges, relative large-magnitude events tends to occur in the deeper level, whereas very shallow seismicity moment is weaker.

In contrast, within the forearc between latitudes 38.5°S and 39.5°S, crustal hypocenters locate at significantly deeper-crustal levels, reaching depths of up to 40 km (*e.g.* epicenters to the west of the Villarrica Lake in Fig. 6.a and 6.c). In general, these events have larger uncertainties and locate outside of the network in areas of predominate 2-D structure (such as a magmatic arc). However, local earthquake tomography studies in the forearc and intra-arc regions between 39° and 40°S do not resolve significant lateral velocity changes for the upper crust (Dzierma et al., 2012b), so the minimum 1-D velocity model with station corrections (Fig. 2) is a good approximation of the 3-D structure (Kissling, 1988). Therefore, we used maximal hypocenter depths from events close to our network (GAP<200) together with the more regional catalogue

from Dzierma et al. (2014) to define the seismogenic layer bottom (SLB). Dzierma et al. (2012 a, b; see for instance cross sections P1 and P2 in Fig. 6 in Dzierma et al., 2012a) show how crustal seismicity observed in forearc locates much deeper than in the intra-arc, describing a convex-like distribution of events. On latitudinal cross-section view (Fig. 6.c), hypocenters delineate a ~120 km long convex geometry for the crustal SLB, which is shallower near the arc-axis, where the LOFS and ATFs are found.
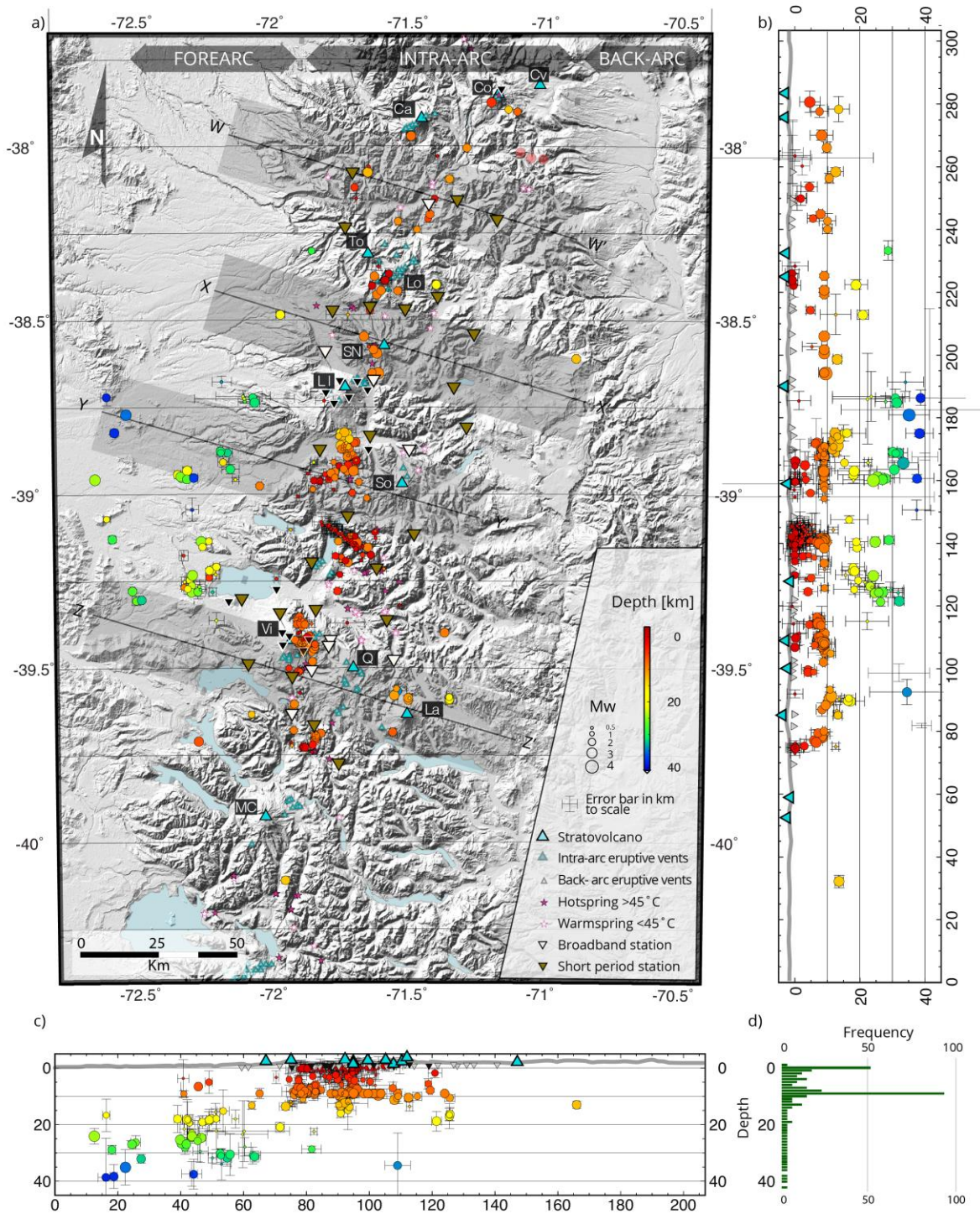
Fig. 6. Southern Andes crustal seismicity. A) Mapview of local seismicity. Hypocenter location uncertainties for each event are indicated with error bars. Main volcanic and geothermal features (Sernageomin 2002; Hauser, 1997) are plotted. Holocene stratovolcanoes: Callaqui (Ca), Copahue (Co), Caviahue Caldera (Cv), Tolhuaca (To), Lonquimay (Lo), Llaima (Ll), Sierra Nevada (SN), Sollipulli (So), Villarrica (Vi), Quetrupillán (Q), Lanín (La) and Mocho-Choshuenco (MC). Quaternary minor eruptive vents are tele-detected and compiled in this study. Digital elevation model (DEM) from STRM30 (https://lta.cr.usgs.gov/SRTM1Arc). Central traces of N74˚W-striking swath cross-sections [W-W' to Z-Z'] presented in Fig. 10 are indicated with black lines. Swath width to scale (gray bands). B) Longitudinal cross section along 71.5˚W. Only events with distances of less than 120 km to the profile are shown. The gray line is the average topographic elevation from the DEM. C) Like "b" but on a latitudinal cross section at 39˚S. d) Histogram (1 km bins) showing hypocenter depths.

Moreover, intra-arc seismicity can be organized into three geographic domains with distinctive geometrical patterns, as shown in Figures 7,8 and 9 and Video S1:

(1) Northern domain (Fig. 7, 37.9°S – 38.8°S). This region contains 51 crustal events with small hypocenter uncertainties (±0.2, ±0.5 and ±0.4 km) in the NS, EW and vertical components, respectively. From south to north, 8 hypocenters locate on the north-eastern flank of Llaima Volcano and surrounding the Sierra Nevada (labelled Ll and SN in Fig. 7), on a plausible NNW-oriented cluster. Two focal mechanisms, including the July 31st 2014 (M_w =3.4) event –largest intra-arc event recorded during the experiment- are coherent with a dominant strike-slip setting with a NE-trending maximum subhorizontal shortening. The M_w 3.4 event occurred at the eastern tip off a ENE-oriented volcanic fissure in the northeastern flank of Llaima Volcano. A single extensional focal mechanism is observed beneath the Sierra Nevada volcano summit. This solution indicates ENE-oriented, steeply-dipping normal fault planes, whose geometry is similar to that of the ENE–striking dike swarm in Sierra Nevada western ridge (indicated as a narrow volcanic fissure in Fig. 7). At Lonquimay Volcano (Lo in Fig. 7), seismicity splits into two ~N20°E and N30°E striking bands, consistent with the northernmost branches of the LOFS (dashed blue lines in Fig. 7; modified from Pérez-Flores et al., 2016). These features occur along strike of prominent morphologic structures, as river incisions and aligned Holocene scoria cones (minor eruptive vents in Fig. 7). Two computed focal mechanisms indicate strike-slip and reverse faulting consistent with NE- to ENE- striking horizontal compression axes, respectively. By integrating surface mapped fault traces and the distribution of hypocenters, ENE- to NE-oriented fault surfaces might dip steeply east, shaping a splay fault array at the northern termination of the LOFS.

(2) Central domain (Fig. 8, 38.8° - 39.3°S). In this segment, we find oblique-to-the-arc striking seismicity clusters, which we describe from south to north:

i. NW- oriented cluster alignment involving the Villarrica Lake (VL), the Villarrica Volcano (Vi) and the Lanin Volcano (La) individual ~NW oriented clusters (Fig. 8.a) is consistent with the trend of the LFZ (e.g. Haberland, et al. 2006). Along this alignment, seismicity progressively deepens west- and eastwards away from the arc-axis, dipping with an angle of ~30° in-line with a rise of the seismogenic layer bottom (SLB) beneath the volcanic arc (latitudinal cross section of Fig. 8b). Towards the west, the forearc hypocenters reach depths of up to ~40 km, whereas beneath stratovolcanoes, depths are less than 13 km. Towards the east, seismicity is sparser, but clearly deepens down to ~17 km, with the exception of one event at 35 (±12) km depth beneath the Lanin volcano. This observation (convex SLB in sectional view) is supported by 107 crustal events located by Dzierma et al., 2012a (events with centered black dots in Fig. 8 a and b). Crustal activity clearly splits from interplate seismicity constrained by Dzierma et al. (2012a, b) who describe a ~30° east-dipping and ~20 km thick subducting slab geometry (Fig. 8). In this overall NW- striking cluster alignment, intense activity (46 events with Mw between 1.1 and 2.5) took place at ~9 km depth underneath the Villarrica Volcano (Fig. 8c) from the 18th to the 23th of April – i.e. forty-five days after the March 3rd, 2015 Villarrica's strombolian eruption, represented as the green dashed line in Fig. 5a and 5b. The NW-oriented seismicity cluster and accompanying computed focal mechanism indicate a dominant sinistral strike-slip regime with E-W±20° oriented maximal horizontal shortening axis (Fig. 8c).

ii. A N60°W-striking micro-seismic sequence in the Caburgua Lake (Fig. 9 and Video S2) reveals a sub-vertical faulting process that took place within 03 successive marked steps. This is documented by peak activity occurring on November 13 to 15 (~68 hours), December 9 and December 16, 2014 (see temporal distribution in Fig. 5.a). Hypocenters distribute at all depth between 9.9 km and -1km depth (*i.e.*

hundreds of meters below the surface in the mountainous sector), being the two more frequent depths ranges: 9.2 to 8.6 km (n=16) and 0.3 to -0.1 km (n=28). Similar to the Villarrica Sequence, narrow seismic alignment and computed focal mechanism delineate a 20 km long transpressional N60˚W left-lateral strike-slip fault with E-W ±20˚ oriented maximum horizontal shortening axis (Fig. 9).

iii. A N50˚E-striking elongated cluster at the north-western flank and basement of Sollipulli Volcano (here called 'Sollipulli cluster'), occurs in close spatial relationship to main fumaroles and surface geothermal activity (Fig. 9). A brief sequence, consisting of 11 NE- aligned events, occurred from the 12th to the 15th of October 2014, with the greatest magnitude event of 1.9 *(Mw)* on November 14th, 2014 09:09:36.7 UTC. A single focal mechanism indicates strike-slip faulting with N-S oriented maximum horizontal shortening axis. In combination with the overall cluster geometry, this would indicate left-lateral strike-slip faulting in a N50E-striking fault. Towards the north, deeper activity is clustered between 12 and 18 km in a NNW plunging cylinder-like cluster. In this sub-domain, cluster orientation can be associated with the LOFS. The latter activity occurring 13 km south from Llaima, and 14 km northwest from Sollipulli stratovolcano summits, has been also reported by OVDAS and analyzed by Mora-Stock et al. (2012). This cluster occurs beneath the town of Melipeuco, in the Allipén valley (indicated with pink diamond in Fig. 9). Our computed focal mechanisms (n=04) in this secondary cluster reveal predominant strike-slip, but also reverse (01 event) faulting with NE-SW (03 events) to NW-SE (01 event) shortening axes (Fig. 9).
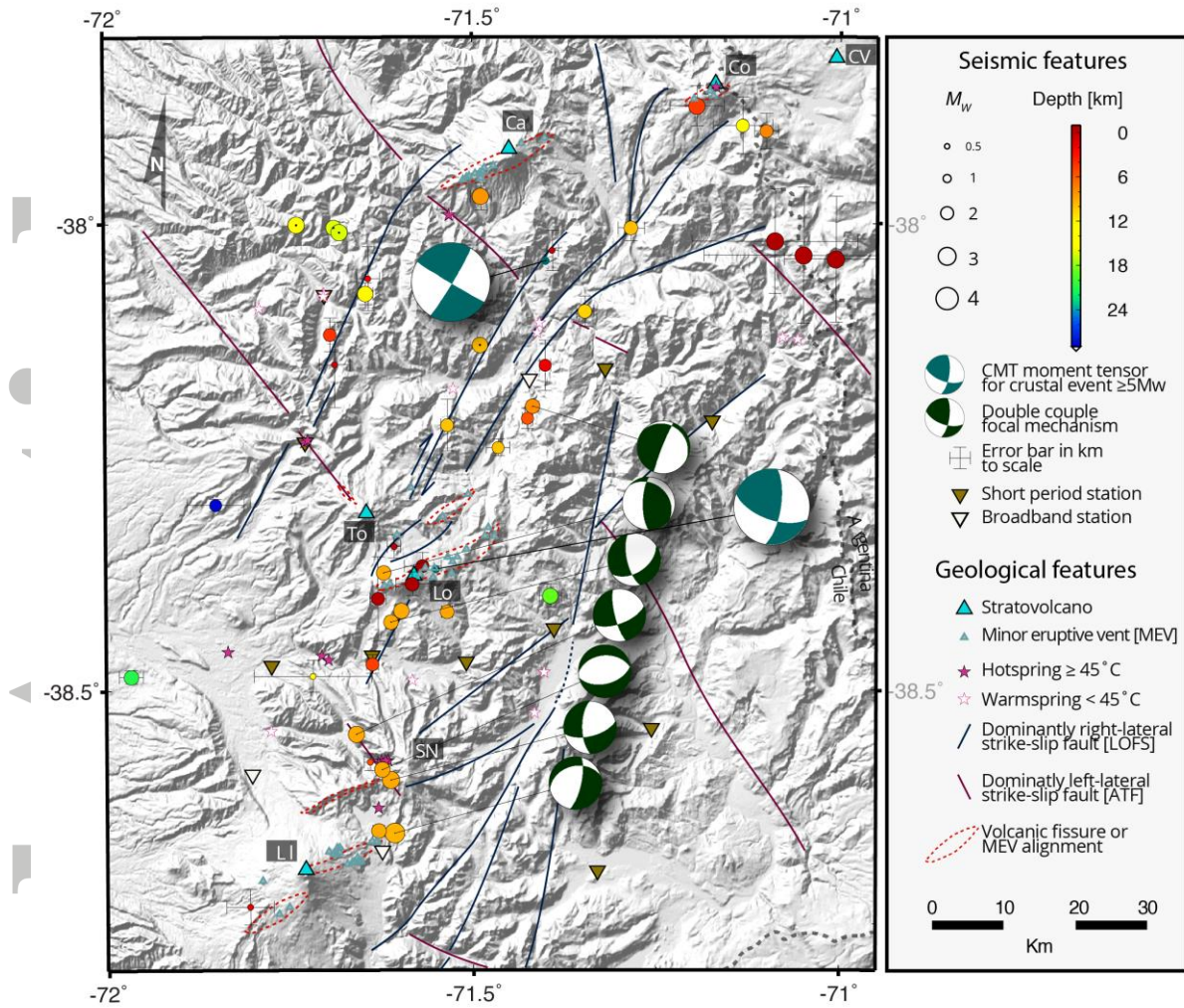
Fig. 7. Crustal seismicity in the northern domain. The four events with centered black dots and absent uncertainty bars are from the seismicity catalog of Dzierma et al. (2012a). Events align along N~30˚E oriented fault branches of the LOFS and long-lived ATF (dashed when inferred; modified from Pérez-Flores et al., 2016). The N30˚W ATF Biobio-Aluminé fault (BBAF) is indicated with purple lines. Multiple minor eruptive vents (MEV) frequently are organized on ENE- to NE-oriented alignments.

(3) In the Southern domain, between 39.5˚ and 40˚ S, events distribute along two ~20 km long sub-parallel N10˚E-trending bands (Fig. 8c). Hypocenters often coincide spatially with surface mapped master branches of the LOFS. A small N-striking elongated cluster can be observed at Liquiñe (Fig. 8c). Two focal mechanisms reported here suggest normal faulting, with NS striking fault planes solutions, or strike-slip with north-south oriented maximum sub-horizontal shortening axis.
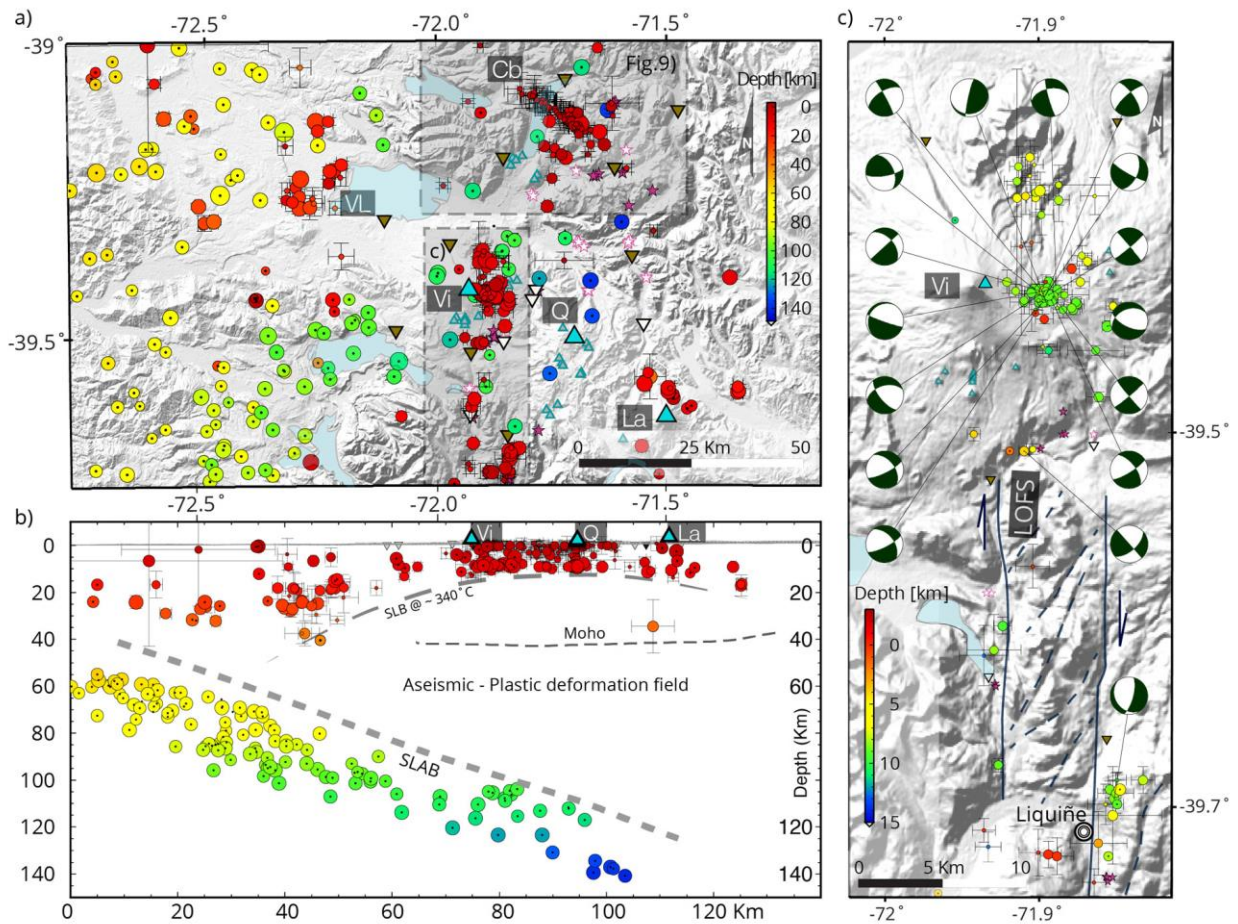
Fig. 8. A) Seismicity distribution of SAIAS catalog (with uncertainty bars) together with the regional catalog from Dzierma et al., 2012a (shown without uncertainty bars and centered-black dots). Hypocenters in red denote crustal events, showing NW-SE aligned clusters, *e.g.* the Villarrica Lake [VL]- Villarrica Volcano [Vi] – Lanin Volcano [La] cluster alignment and Caburgua Lake sequence [Cb]. Geological and seismic features follow the same symbol criteria than figure 7. b) Latitudinal cross section with 25 km swath width to both sides. Vertical exaggeration is 0.5. Our data (events in colored dots with uncertainty bars) is confronted to the SFB-Kiel project data from 2009 for the fore-arc (events in colored dots and black centered dots). Crustal seismicity depicts an upwelling shape for the bottom of the crustal seismogenic layer (red dots) at a theoretical 300˚C isotherm (e.g. Stesky, 1975; Scholz, 2002). For reference, deeper events of Dzierma et al. (2012a) are plotted delimiting the interplate seismogenic zone (Wadati-Benioff zone). A referential Mohorovicic discontinuity is outlined based on receiver functions (Yuan et al., 2006) and our local velocity model (white dashed line). c) Inlet indicated in 'a'. Hypocenter distribution and computed focal mechanism for shallow events occurred within the Villarrica volcanic edifice – i.e. a NW oriented cluster southeast of the summit and another sparse cluster north of the summit - and along major N10˚E oriented fault branches of the LOFS. Note different depth color coding for panels a and c. Inlet of southernmost portion of figure 9 is indicated.
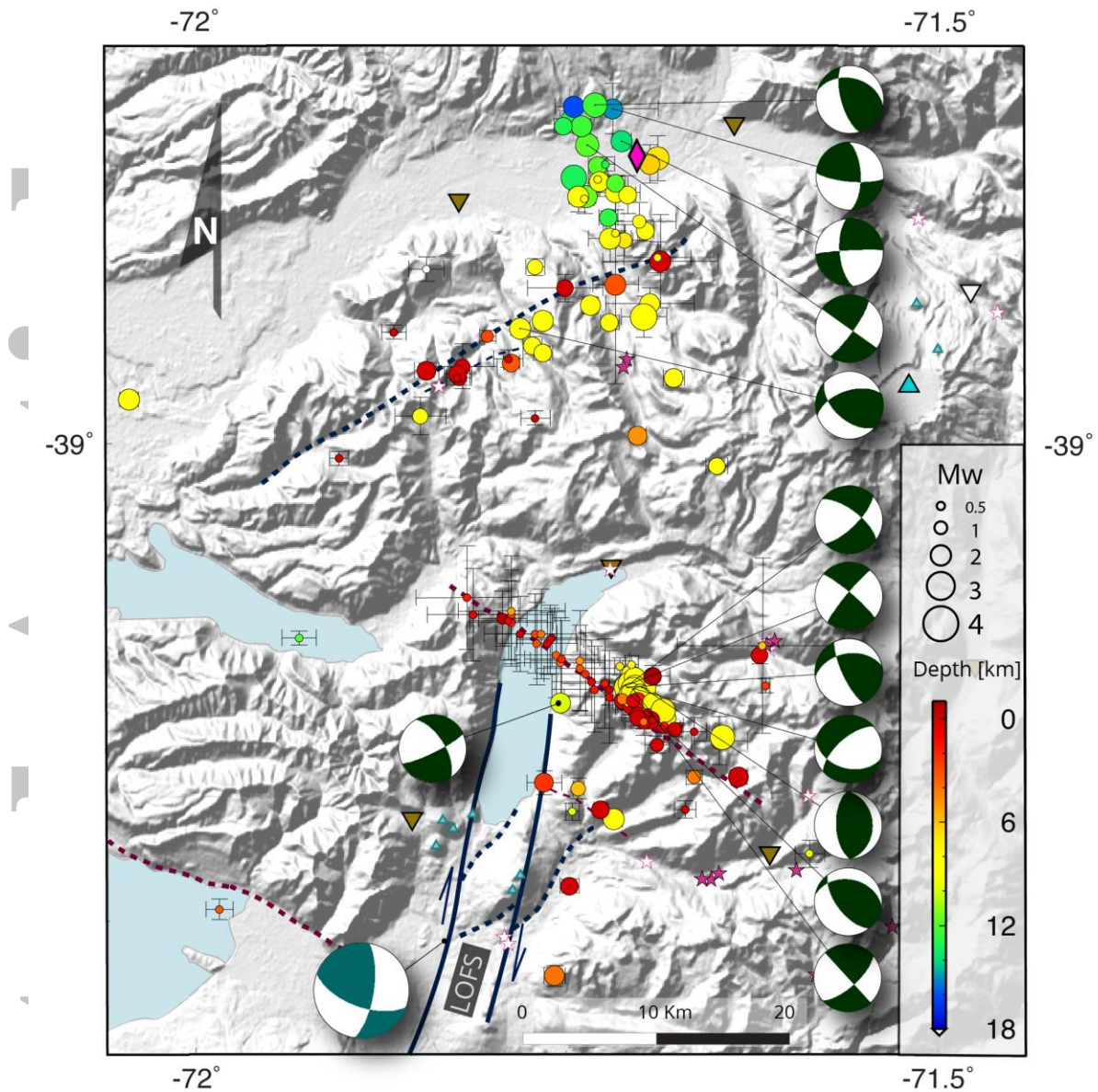
Fig. 9. Close-up map view with seismicity of the central domain (location of this map is shown in Figure 8.a). Computed focal mechanisms are indicated in dark-green and white, whereas moment tensors for the *Mw* 5.2 on 24/02/1989 at 15 km of depth (gCMT) is plotted in light-green and white. The Melipeuco town is indicated with a pink diamond. Other symbols follow the same criteria as previous figures.

5 Discussion

In the south-central Andes, along the LOFS northern termination, intra-arc seismicity is a physical phenomenon enabling the identification of current deformation/stress states and associated faulting. Intra-arc seismicity can clearly be discriminated from crustal forearc seismicity based on the following observations: (i) its shallowest typical hypocentral depth, ranging from ~-0.2 to ~12 km (Fig. 6.b,c,d and 8.b and 10; (ii) its predominant strike slip kinematics; and (iii) its geographical occurrence on or close-to long-term crustal faults (LOFS and ATF) and/or Quaternary eruptive centers and geothermal areas (see Fig. 6 for regional context and Fig. 7, 8 and 9 for local spatial relations). In turn, forearc crustal

seismicity is mostly localized on ATF (e.g. Pichilemu Fault, Lanalhue Fault Zone) and might be continuous to the intra-arc, as the LFZ follows the Vl-Vi-La NW-striking seismic cluster alignment. This point will be further addressed later.

As it is widely accepted, the *b-value* is a constant for the Gutenberg-Richter (G-T) relation that measures the ratio of large earthquakes over small ones. Therefore, the *b* value is related to the fractal dimension of faulting (e.g., Aki, 1981; Turcotte, 1997). Globally, the *b-value* is frequently found between 0.8 and 1.2 for a wide variety of active tectonic regions (e.g. Utsu, 2002). Our estimates yield to a *b-value* of 1.11 (data fits the G-T relation up M_{co}; Fig. 4), which is coherent with a tectonic origin of the intra-arc seismicity. Additionally, the tectonic nature is confirmed by the dominant stick slip behavior of active intra-arc faulting, deduced from clear and distinctive *P*- and *S*- wave onsets for most recorded events (Byerlee and Brace, 1968). Recently, similar b-values and faulting mechanism behavior have been documented for crustal seismicity in the pre-cordillera of northern Chile (Salazar et al., 2017). Although, crustal composition, fluid presence/absence and crustal thickness might differ from northern to southern Chile, we can support that the first order control for crustal seismicity derives from tectonic forces associated with the overall oblique convergence setting.

5.1 The frictional-plastic transition in the intra-arc region

Based upon our observations, the thinner and shallower intra-arc seismogenic zone of the SVZ may be the most favorable crustal domain to accommodate frictional strain in the overriding South American plate. This is consistent with an earlier observation made by Barrientos et al. (2004) for Central Chile (33°- 35°S) indicating a higher rate of crustal seismicity within the arc, in comparison to the observed activity in the forearc and back-arc regions. This idea may also be in harmony with an enhanced thermo-mechanical weakness of a heated crust, as originally proposed (Fitch, 1972, Tikoff and Teyssier, 1994, De Saint Blanquat et al., 1998). Furthermore, because seismic velocities decrease with increasing temperature and deformation (Griffin and O'Reilly, 1987; Sibson, 1984; Sibson, 2002), a heated and fractured crust might explain the relatively low velocity structure in the upper intra-arc crust (Fig. 3a) when it is compared to other 1D crustal velocity models calculated for Southcentral and Central Chile (Haberland et al., 2006, Lange et al., 2007). Thus, arc-orthogonal geothermal gradients may significantly influence the brittle architecture of the overriding plate, enhancing faulting where the crustal seismogenic layer is thinner.

In quartzofeldespatic crust, greenschist metamorphism or quartz plasticity onsets at around ~300°C (Stesky, 1975). This sub-solidus crustal boundary marks an inflexion point of crustal strength (Scholz, 1988; Sibson, 2002). Thus, in continental margins with an active volcanic arc, the vertical transition from a frictional faulting domain to quasi-plastic shearing may be significantly deeper in regions tens of kilometers away from the arc axis. Moreover, i*n situ* studies in northern Japan combining local seismicity and direct temperature measurements of geothermal-boreholes in granitic crust, indicate that the SLB in this region corresponds to the 380°C isotherm (Suzuki et al., 2014). They correlate this temperature with depths for the thermal conduction/convection transition. Whereas the maximum strength zone would be consistent with the 340°C isotherm, where the brittle-ductile transition is defined (Suzuki et al., 2014). Based on our data, quasi-plastic mechanical behavior of the crust would be expected for depths below the convex envelope of the crustal seismogenic layer bottom, as seen in section (data in Fig 8b, Fig. 10 and schematized in Fig. 11). This feature is conspicuous between latitudes 38.5°S and 39.5°S where crustal seismicity is organized within a NW-oriented seismic volume, consistent with the NW-striking Lanalhue Fault (e.g. Haberland et al., 2006), NW-aligned clusters (VL-Vi-La) and with the NW oriented

Caburgua crustal seismic sequence (Fig.8a, 8b and Video S1). A similar shape of the SLB, can be observed to the kilometric-scale in active geothermal fields of northern Japan, where high resolution passive seismic mapping, define local and abrupt shallowing of the SLB at very high geothermal gradients (Suzuki et al., 2014).
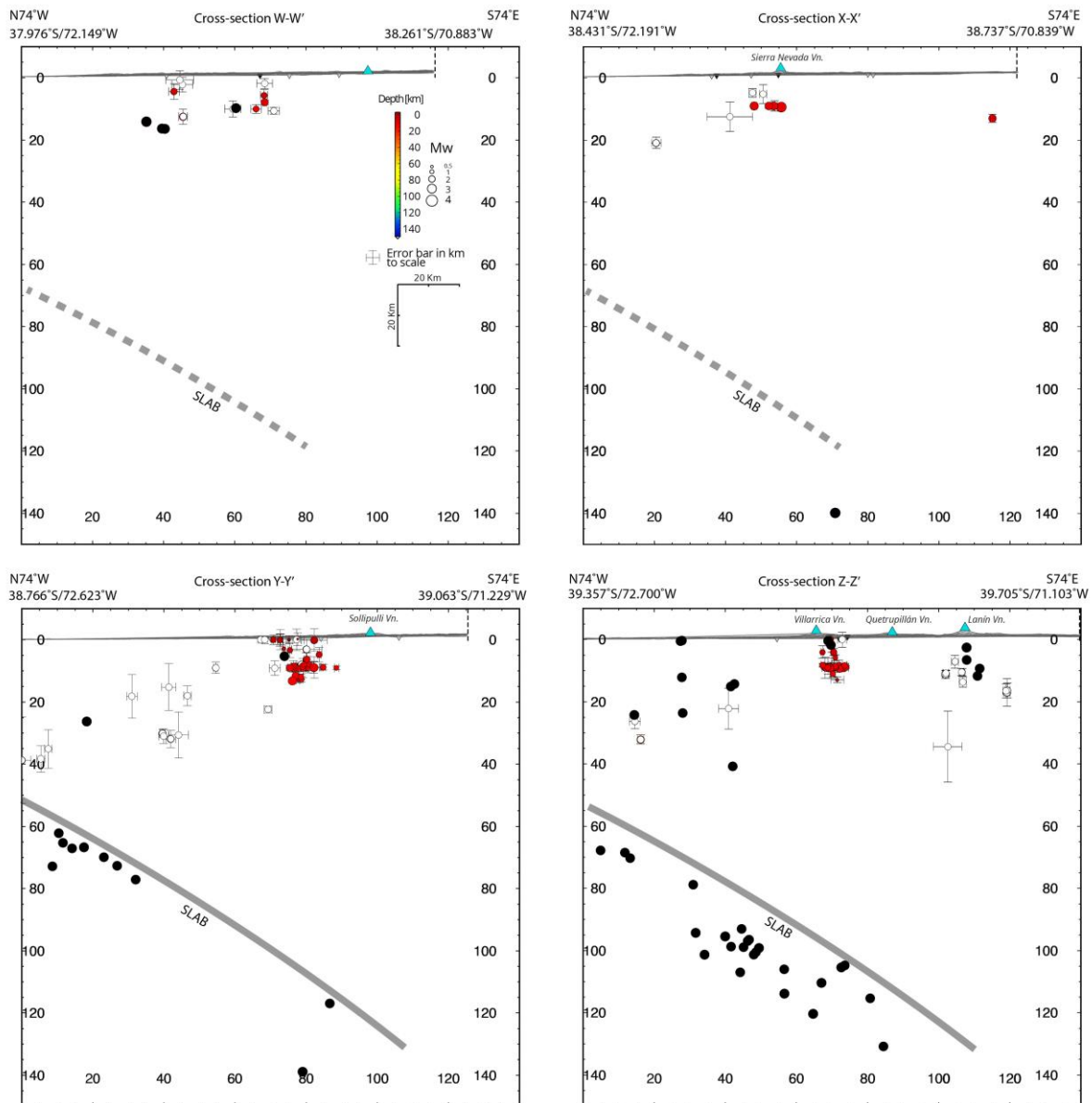

Fig. 10. Cross-sections (perpendicular to the LOFS and SVZ) showing the local seismicity, together with the regional earthquake catalogue from Dzierma et al. (2012). Location and swath of the profiles are shown in Fig. 6.
Local events are shown with uncertainties. Events close to the network (GAP<=200°) are indicated with colour circles. Seismicity far outside the network (GAP>200°, poor constraint depths) are shown in white circles, and are not used for interpretation. Events from the earthquake catalogue from Dzierma et al. (2012 a, b) are plotted as black circles. Strato-volcanoes are indicated with light-blue triangles and seismic stations are shown with inverted triangles (black=broadband, white=short-period). Note that vertical and horizontal scales are equivalent. Slab geometry (grey line) inferred from interplate seismicity (Dzierma et al., 2012a) is dashed where no data is available and is projected from southernmost cross-sections. Topographic relief is projected from SRTM 30 data. Northernmost swath cross-section (W-W') is 20 km wide, whereas the other three (X-X', Y-Y' and Z-Z') are 24 km wide.

Similar crustal geometries have been observed for the Central Andes. For example, Farías et al. (2010) associated the west-dipping hypocenter distribution in Central Chile (33°-35°S) with the shape of the continental margin ~400°C isotherm, which was earlier defined at a more regional scale by Yañez and Cembrano (2004). Farías et al. (2010) interpreted this structure as an east-vergent, low angle thrust that would play a major role in the Andean mountain building. If this constitutes the main crustal architecture of the Chilean Southern Andes, the forearc seismicity should be decoupled from the intra-arc seismicity and most of the hypocenters should be distributed close to the base of the SLB. The observed seismicity should then define a low angle, west-dipping seismogenic plane and dip-slip focal mechanism would be expected. Nonetheless, activity in the forearc between 38.5°S and 39.5°S (ATF) occur in a wide depth range (0-40 km; Fig. 8b) and focal mechanisms are mostly strike-slip (Haberland et al., 2006), indicating a prominent NW oriented Andean-transverse deformation system. The latter could be defined as a NW oriented crustal volume that includes the Lanalhue Fault (Glodny et al., 2008, Haberland et al., 2006, Melnick et al., 2009), the VL-Vi-La seismic cluster alingment and the Caburgua seismic sequence. If the upper crust is detached by a subhorizontal convex layer (e.g. SLB), then the partitioning would not show predominantly in the magmatic arc because the tectonic forces in the forearc would be accommodated close to the SLB and not in the whole brittle-crust section, as it is revealed by ours and others seismic experiments (Dzierma et al., 2012 a, b; Haberland et al., 2006). So, what is the source, then, to the conspicuous observed strike-slip faulting? We consider that the partitioning of convergence between subduction and strike-slip movement of the forearc slivers constitute a simple and more straight-forward explanation to the observables, and that the low angle detachment alternative is at least equivocal in this segment of the Andes (38°S-40°S).

Recent local seismicity studies in northern Chile forearc (Bloch et al., 2014; Salazar et al., 2017) demonstrated an analogue and marked convex shape of the SLB boundary around the West Fissure Fault System (WFFS) and Northern Chile volcanic arc. By contrasting hypocenters to heat-flow density models, Salazar et al. (2017) observed that crustal seismicity is clearly organized above the 350°C isotherm (Springer, 1999). The latter, down to ~60 km depth in the forearc-slab boundary, progressively shallows up to ~15 km beneath the active volcanic front, describing a convex geometry in line with the maximum depth of crustal events. In turn, in the southern Central Andes (32° - 33.4°S), Nacif et al. (2017) show similar hypocentral depths beneath the volcanic front (< 12 km). Integrating EHB Bulletin Catalog data, this author, indicates also how foreland/back-arc seismic activity locates progressively deeper to the east, down to reach the continental Moho (~ 50 km depth), about ~550 km away from the trench. In contrast with Farías et al., (2010) interpretation of an east-vergence major crustal thrust, and in agreement with Salazar et al. (2017), we suggest that a first-order control of the convexity and thinning of the SLB in Northern and Southern Chile volcanic arcs is related to a critical isothermal envelope limiting the frictional deformation field in depth. The geometry of this rheological transition might be caused by thermal diffusion of active magmatic heat sources along the arc, independent of inherited fault geometries, but probably from fluid content and availability. Additionally, reflection seismic studies in Northern Chile define two sub-parallel west-dipping bright spots between 15 and 40 km of depth (Yoon et al., 2003; Yoon et al., 2009). These structures are consistent in geometry and position with the SLB defined by Bloch et al., (2014) and Salazar et al. (2017), as well as with the 350°C isotherm (Springer, 1999). Towards the arc front, where activity is shallower (15-20 km depth) these structures have been correlated to the Altiplano low-velocity zone, the one has been proposed to demark the brittle-plastic transition in this region (Wigger et al., 1994; Yuan et al., 2000). In summary, for the Southern Andes, the SLB might delineate a major rheological boundary between upper and mid-crustal levels, similarly as was proposed

by Koulakov et al. (2006) and Bloch et al. (2014) for the Andes orogeny in northern Chile. For this segment of the Andes, we assume that the SLB temperature should be within the temperature range of 300°-380°C, considering a quartzofeldespatic crust mainly formed by Tertiary granitoids and volcano-sedimentary rock successions (refer to Fig. S1 in supplementary information).

However, the SLB shape might not only be controlled by the geothermal gradient, but by the strain rate and the presence of crustal fluids, diminishing rock strength to failure. Long-term geologic data shows that continental margin high-strain domains are mostly localized along the Miocene-Present day volcanic arc and/or at long-lived ATF (*e.g.* Rosenau et al., 2006; Glodny et al., 2008; Cembrano and Lara, 2009; Pérez-Flores et al., 2016; among others). If the current strain rate is indeed higher in the volcanic arc domain, the SLB should be deeper than that of the forearc and foreland regions given a constant geothermal gradient, which is something not supported by our data and that of previous work (e.g. Nacif et al., 2016; Salazar et al., 2017). Therefore, although strain rate in the volcanic arc is higher, the effect of heat flux and associated higher geothermal gradient largely overcomes that of strain rate. ATF can provide key evidence in favor of the role of differential geothermal gradient on the depth of seismicity because they run across the forearc and arc regions. For instance, the maximum seismicity depth recorded along the strike of the LFZ goes from ~40 km in the forearc to ~12 km within the arc (Haberland et al., 2006; Dzierma et al., 2012a; in addition to our data). This strongly supports the hypothesis that differential geothermal gradient is one first order control on the maximum depth for seismicity on Andean crustal faults.

Regarding the influence of crustal fluids, it is well known their effect on reducing effective stresses and promoting failure. Regions with enhanced fluid pressure at all crustal levels will tend to have a deeper SLB. If fluid pressure is not evenly distributed with depth, the effects are difficult to generalize, because they will depend on local conditions. In the Southern Volcanic Zone, there is widespread evidence for upper crustal fluid flow in the form of magma and/or hydrothermal fluids/hot springs (i.e. NE-oriented electrical conductor; Brasse et al., 2008). This would probably have an effect on enhancing faulting and seismic activity in the uppermost crust (~0-2 km); effects at higher depths are difficult to constrain at regional scales. A local example of this, however, will be discussed when addressing crustal fluid-related seismicity below.

5.2 Strain partitioning and compartmentalization

Intra-arc seismicity provides fundamental insights on how transpressional deformation partitions, transfers and compartmentalizes within the overriding plate. The results of our brief time-window (~16 months) experiment, however, is reasonably consistent with most of the main tectonic features already documented through different approaches/methodologies (*i.e.* structural geology, numerical modelling and geodetic studies) on the long-term pattern of crustal strain within intra-arc regions. Tikoff and Saint Blanquat (1997) have stated that syn-magmatic strike-slip partitioning may accommodate within margin-parallel strike-slip mylonitic and cataclastic domains. In turn, a combination of strike-slip and reverse faulting in the forearc and foreland/back-arc regions may accommodate both margin-parallel and margin-orthogonal components during one interseismic stage of the subduction earthquake cycle. However, few studies (La Femina et al., 2002; Lange et al., 2008; Stanton-Yonge et al., 2016; Pérez-Flores et al., 2016; Salazar et al., 2017), which include detailed observations, yield a more complex picture regarding the way by which the margin-parallel component accommodates within the intra-arc. In fact, it might be entirely accommodated by margin-oblique faults (*e.g.* bookshelf faulting in Central Andes volcanic arc; La Femina et al., 2002); or strain might distribute within variable orientations and with a

wide kinematic range, as deduced from focal mechanisms in Northern Chile, with statistically dominant oblique-slip kinematics, with substantial strike-slip component (Salazar et al., 2017). The observations include both the long-term and present-day interplay between margin-parallel and transverse fault zones, which in turn are spatially associated with volcanism and hydrothermal activity (*e.g.* Cembrano and Lara, 2009; Sánchez-Alfaro et al., 2013).

The continental continuous crustal deformation (displacement) model for Latin America (VEMOS2015 model with spatial resolution of 1˚ x 1˚; Sánchez and Drewes, 2016) inferred from GNSS (GPS+GLONASS) measurements gained after the 2010 Maule megathrust earthquake, indicates how the effect of the Maule earthquake changed the surface kinematics of a large continental area (30˚-45˚S), particularly in the Andean region. The model indicates, that before the earthquake, the strain field showed a strong west-east compression between 38˚S and 44˚S (roughly parallel to the convergence vector) whose magnitudes diminish with distance from the subduction front. After the earthquake, and until the end of the measurements in 2015, the larger horizontal compression was documented between 37˚S and 40˚S, with a N30˚E oriented axis. The authors predict that the present-day deformation (valid for the period 2010-2015) caused by the Maule earthquake, might extend between 30˚S and 45˚S (Sánchez and Drewes, 2016). However, no increase in seismicity was observed along the magmatic arc after the Maule earthquake (Lange et al., 2012; Mora-Sock et al., 2011). Similar observations have been made for other subduction regions (e.g. at Sunda subduction zone the 2004, 2005, 2007 and 2012 earthquakes where not followed by higher seismicity rate along the Sumatra Fault, although predicted by Coulomb stress models (e.g. McCloskey et al., 2005; Pollitz et al., 2006). As a general approach, the N30˚E horizontal shortening derived from VEMOS2015 would be in kinematic coherence with the numerical modelling implemented by Stanton-Yonge et al. (2016), however the far field stress tensor differs from the N30˚E horizontal shortening. The latter study, computes and compares the expected displacements and kinematics on long-lived crustal faults in Southern Andes (LOFS and ATF) for both, co- and interseismic stages of the subduction earthquake cycle. Beside local anomalies induced by post-seismic deformation and heterogeneous locking distribution, the interseismic model fits well GPS data (Wang et al., 2007; Moreno et al., 2011 among others). The model yields right-lateral slip with a maximum rate of 3.5 mm/yr on the Eastern Master of the LOFS (involved in our study area) and oblique sinistral-reverse slip for NW striking ATF with the potential to accommodate a maximum slip rate of 1.4 mm/yr. In turn, ENE striking fault would display dextral slip along strike at a maximum rate of 0.85 mm/yr. This partitioning pattern in the intra-arc region is in agreement with the faulting geometries and with several strike-slip and compressional focal mechanisms, with NE to NS maximum horizontal shortening here presented (Figs. 7, 8 and 9).

Depending on the epicentral distance and position, for a coseismic phase, in turn, we would expect an inversion of the strain pattern and fault kinematics here described. As presented by Stanton-Yonge et al. (2016), coseismic deformation field resulting from the 2010 earthquake induced normal-sinistral slip along the LOFS with a maximum slip at its northern termination. Accordingly, NW-striking faults (in the latitudinal range of the earthquake rupture area) would switch to dextral-normal slip, and ENE oriented faults, to sinistral slip. Unfortunately, no coseismic crustal earthquake has been reported for such arc-parallel or arc-oblique faults, apart from the post-seismic, NS-striking right-lateral strike-slip El Melado 6.0 *(Mw)* earthquake (Fig.1; Cardona et al., 2015). Nonetheless, Cifuentes (1989) reports a *Ms* ~7.5 coseismic crustal earthquake (June 6th 1960, *i.e.* 15 days after the 1960 Valdivia megathrust *M* 9.5 earthquake) on top of the surface trace of the LOFS southern termination. Previously, Kanamori and Stewart (1979), proposed right-lateral slip on a N80˚E oriented fault plane for this event. Although this solution is poorly constrained, it suggests a

NW- oriented horizontal coseismic compression axis and NE- oriented horizontal coseismic extension axis, which are in accordance with the coseismic strain field proposed by Stanton-Yonge et al. (2016). However, expected coseismic activity within the intra-arc seismogenic zone might occur in compatibility and dependence of the coseismic strain field and intra-arc faults geometries.

Spatial and spatio-temporal analyses of our data reveal variable faulting styles taking place predominantly within the uppermost 12 kilometers of the magmatic arc (schematized in Fig. 11). Predominant NNE and subordinate NE-striking faults of the LOFS, in addition to the NW-striking ATF, shape the active intra-arc schizosphere seismogenic fabric. For instance, high angle, east-dipping mapped faults (Lolco Fault, Pérez-Flores et al., 2016), and slightly east-shifted N20˚E to N30˚E striking hypocenter alignment, configure a splay fault array at the northern termination of the LOFS (Fig. 7). In turn, the central zone of the study area is characterized by Andean transverse faulting. This is evident from isolated events and clusters aligned on a >100 km long NW striking band, extending from the Lanin Volcano towards the forearc (*i.e.* VL-Vi-La in Fig. 8a). We propose that such Andean transverse strain domain is controlled by a long-lived (pre-Andean) NW-striking faults with sinistral-reverse kinematics as the dominant shortening pattern deduced from focal mechanism of the Vi cluster. On a smaller scale, kinematically compatible activity on tens-km long ATF is prompted on narrow NE- (e.g. Sollipulli cluster) and NW- (e.g. Caburgua cluster) striking intra-arc seismic fault zones. Temporal evolution, geometry and kinematics of micro-seismicity at the Caburgua Lake, could be related to a swarm-like behavior (Fig. 9). The southernmost zone reveals a spatial distribution of crustal seismicity in association with major branches of the LOFS. In particular, the Liquiñe, Villarrica and Caburgua clusters, might be consistent with fault geometries and kinematics of second order faults of the LOFS and ATF with Holocene neotectonic activity, as suggested from geomorphic analysis by Melnick et al. (2006b) and Astudillo et al. (2018). Detailed and focused paleoseismicity studies in such key sites (clusters) are needed in order to better understand the LOFS and ATF Quaternary slip rates.

Kinematic solutions estimated from seismic source radiation patterns (*i.e.* computed focal mechanisms on Figures 7, 8 and 9 and on Table S2) confirm a prevailing ENE to WNW- instantaneous maximum subhorizontal compression, and local NNE-SSW to N-S compression. The former findings are largely consistent with the long-term deformation recorded by structural geology analysis, and are slightly rotated from the few gCMT (*Mw* ≥5) moment tensors (Fig. 1, 7 and 9). The shortening axes are in turn more coherent with the N30˚E post-seismic shortening axes proposed by the VEMOS2015 model (Sánchez and Drewes, 2016). However, local NNE-SSW to N-S compression solutions, as well as few normal faulting focal mechanisms (*i.e.* vertical maximum shortening) on subsidiary faults of the LOFS, such as the ones at the Sierra Nevada Volcano and Liquiñe clusters (Fig. 7 and 8.c, respectively), might be associated with heterogeneous strain accommodation on damage zones neighboring major faults. It is known, from self-similarity and scaling-parameters studies on fault zones (system that is similar to a part of itself) that faults and related damage zones are created by scale-invariant mechanisms (Jensen et al., 2011; Savage and Brodsky, 2011; among others) and that collateral damage zones may host diverse geometries and kinematics because of rotating blocks, media anisotropies (e.g. healing of previous faults generating buttress boundaries) and/or by stress variations on fault intersections (Kim et al., 2004; Gratier, 2011; Iturrieta et al., 2017). All above-mentioned is consistent with an overall strain partitioning along the arc strike compartmentalized into margin-parallel and Andean-transverse fault domains. Major along-strike changes can be visualized on cross-section of Fig. 6b and Video S1.

Small-magnitude focal mechanisms are expected to be associated either with small displacement along main fault branches, or alternatively to restricted surfaces on subsidiary faults. The former is in line with the natural varying seismic style and asperity sizes along fault strike (e.g. Sibson, 2002). The latter may explain the local clock-wise rotated shortening axes due to slip on subsidiary faults. The experiment resolution is not high enough to specify the source nature of such small magnitude events. However, by considering fault outcrop scale observations, it is reasonable to assume slip on smaller-scale subsidiary faults, as those analyzed by structural geology studies such as those of Lavenu and Cembrano (1999), Rosenau et al. (2006), and Pérez-Flores et al. (2016).
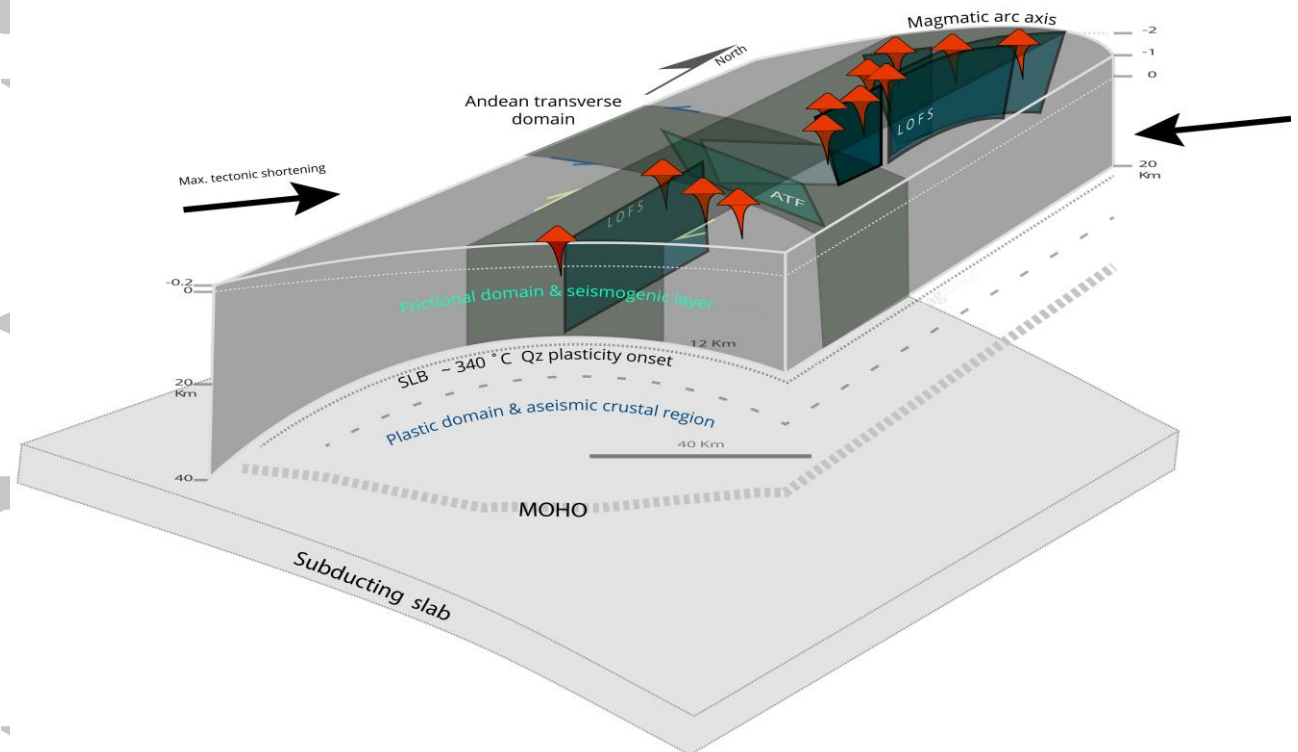
Fig. 11. Conceptual model of crustal seismogenic layers along a magmatic arc. The cartoon includes high frictional strain domains (LOFS and ATF; olive-gray volumes), where expected fault geometries and kinematics respond to the regional shortening axis (black vectors). Strato-volcanoes are represented with the red triangles.

Based on receiver functions analysis, Yuan et al. (2006) resolve the continental Moho beneath the Southern Andes. The Moho is described as a continuous envelope that is deeper beneath the magmatic arc and orogenic front (~45 to 40 km), becoming progressively shallower towards back- and forearc regions (30 – 20 km). The Vp and Vs velocity increment that we see at 35 and 40 km in our minimum 1-D velocity model (Fig. 3a), is in line with the regional Moho depth from Yuan et al. (2006).

5.3 Fluid-related seismicity and the Villarrica 2015 eruption

No clear volcano-tectonic activity has been determined by the present study. However, clustered seismicity, as the one reported between Llaima and Sollipulli volcanoes, might be fluid-related (Fig. 9, northern and deeper cluster). In particular, this site of activity has been previously reported by OVDAS and analyzed by Mora-Stock, et al. (2012). The authors suggest a strong fluid-depend seismic component, as deduced from low frequency events. In particular, this cluster represent the deepest intra-arc activity here reported. This particular cluster - up to 6 km deeper in comparison to the more frequent ~9 km maximum

depth (SLB) along the intra-arc strike -, might be related to deeper-seated hydrofracturing, as a consequence of effective stress reduction, rock-strength weakening and failure (e.g. Cox 2010).

Usually, individual moderate shallow earthquakes occur as localised shear dislocations which do not lead to displacements over the entire surface of an existing geological fault; in turn, seismic faulting may act as a pumping mechanism whereby individual seismic events are capable of moving significant quantities of crustal fluids (Sibson, 1975). Along the south-central Chile arc-strike, an important fraction of the seismicity (98 events, *i.e.* 27% of our catalog; Fig. 6d) locates in the uppermost 4 kms of the crust. For instance, the brief timespan, intermittent and very shallow micro-seismicity observed at the Caburgua NW-striking cluster, might be related to episodic fluids circulation, that could be retaled to sporadic permeability enhancement and seismic swarm-like behavoir.

No evident precursory seismic activity can be linked to the Villarrica strombolian eruption that occurred on March 3rd 2015 (OVDAS, 2015; Naranjo, 2015). Furthermore, we report only 6 events in a 40-day window before the eruption, absence of co-eruptive seismicity, and only 11 events in the following 40-days (Fig. S4). We carefully rechecked the seismograms for 20 days before and after the eruption for small magnitude events, but could not find events which were not previously detected during the catalog creation. Normally, volcano-tectonic pre-eruptive seismicity respond to spatio-temporal evolution of magma-filled cracks expected to be caused by: 1) hydro-fracturing (Aoki et al., 1999; Gudmundson, 2011); 2) faulting linkage between offset dikes (Hill, 1977) or 3) lateral micro-faulting in wall-rock as a mechanical response to stress changes induced by dike inflation (Roman, 2005; Roman and Cashman, 2006). Since no clear seismicity is found prior to the Villarrica 2015 eruption, none of the processes could be associated with the eruptive cycle. Curiously, forty-five days after the Villarrica eruption, an intense seismic sequence took place at around 9 km depth (See Fig. 5a and Fig. S4 to see the increment of number in time and Fig. 8c for detailed observation of the cluster distribution). Strike-slip focal mechanisms and hypocenters describe a NW oriented ellipsoidal cluster, located 2 km to the south-east of the eruptive vent. We speculate that in this position, aseismic (or not detectable by our network) feeder dikes may have been injected. We interpret this particular seismic sequence as an effect of transient, thermo-dependent seismogenic properties of the upper intra-arc crust, where post-eruption micro-cracking and faulting might occur, induced by the reduction of confining stresses due to cooling and contraction of the rock mass. Similar magma-wall-rock behavior has been suggested for small double, and non-double couple earthquakes in Reykjanes, Hengill and Krafla volcanic systems of the accretionary plate boundary in Iceland (Foulger and Long in Gasparini et al., 1992). After the post-eruptive seismic sequence at Villarrica in April 2015, seismicity would have recovered the regional background activity level (Fig. S4). However, no records are available after the 13th of June 2015, the completion date of the experiment. The lack of notable seismicity rate changes after the eruption in March 2015 indicates that seismicity is not a reliable precursor for Villarrica volcano.

5 Summary and Conclusions

In this study, we present moderate to small magnitude seismicity ranging from M_w 3.6 to M_w 0.6, of a 16 month-long natural seismicity experiment. It is the first network to cover the northern termination of the Liquiñe-Ofqui Fault System at a regional scale, and provides high resolution for local earthquake detection and localization. The seismicity catalog consists of 356 crustal events, coherent with the bulk long-term tectonic construe from

structural geology analysis for this segment of the Andean orogeny. Combined interpretations from geometric and kinematic analysis can be summarized into three major outcomes.

1. Frictional strain in the intra-arc region is compartmentalized into geometrically and kinematically distinctive latitudinal subdomains. In the northernmost portion of the LOFS (37.8°-38.8°S), seismic faulting is consistent with the long-term record of brittle deformation. Main NNE-oriented branches of the LOFS give way to a splay fault array, along which minor eruptive centers, stratovolcanoes and geothermal surface expressions are placed. A central zone (38.8°-39.6°S) is dominated by Andean transverse active faults, alternating NW- (*e.g.* Caburgua sequence, VL-Vi-La seismic cluster alignment) with NE-oriented faulting. In the southernmost sector of the study area (39.6°-40.1°S), margin-parallel faults accommodate most of the strike-slip component of the partitioned bulk strain.

2. The latitudinal convexity (as seen in WNW-ESE cross sections) and 30° west dip of the SLB in Southern Andes between latitudes 38.5°S and 39.5°S, is in-line with a geothermal gradient exerting a first-order longitudinal control on the depth of the frictional-plastic transition. From a geometric and linear extrapolation, we suggest that the geothermal gradient is at least three times higher in the arc-axis than in the forearc. Consequently, a higher geothermal gradient and thinner fractured crust in the arc-axis may enhance a feedback loop among frictional strain, permeability increase and convection conditions for shallow fluids to flow and/or emplace.

3. The Villarrica volcano strombolian eruption on March 3rd, 2015 did not have a significant pre-, syn- or post- eruption seismicity. However, an intense sequence, took place 45 days after the eruption at ~9 km depth in a NW-elongated cluster from the summit towards the southeast. We argue that this activity may have been induced by feeder dike cooling and contraction.

Acknowledgments

References

Acocella, V., and F. Funiciello (2010), Kinematic setting and structural control of arc volcanism, *Earth Planet. Sci. Lett.*, doi:10.1016/ j.epsl.2009.10.027.

Agurto, H., A. Rietbrock, S. Barrientos, K. Bataille and D. Legrand (2012), Seismotectonic structure of the Aysén Region, Southern Chile, inferred from the 2007 Mw 1⁄4 6.2 Aysén earthquake sequence, *Geophys. J. Int.,* 190, 116-130, doi:10.1111/j.1365-246X.2012.05507.x.

Aki, K. (1981), A probabilistic synthesis of precursory phenomena, in Simpson D.W. and P.G. Richards, Earthquake Prediction: An intenational review, Maurice Ewing Ser., 4, 566-574.

Angermann, D., J. Klotz, and C. Reigber (1999), Space-geodetic estimation of the Nazca-South America Euler vector, *Earth Planet. Sci. Lett.*, 171(3), 329–334, doi:10.1016/S0012-821X(99)00173-9.

Aoki, Y., P. Segall, T. Kato, P. Cervelli, and S. Shimada (1999), Imaging magma transport during the 1997 seismic swarm off the Izu Peninsula, Japan, *Science*, 286(5441), 927-930, doi:10.1126/science.286.5441.927.

Arancibia, G., J. Cembrano and A. Lavenu (1999), Transpresión dextral y partición de la deformación en la Zona de Falla Liquiñe–Ofqui, Aisén, Chile (44–45˚S), *Rev. Geol. Chile* 26, 3–22, doi:10.4067/S0716-02081999000100001.

Aron, F., J. Cembrano, F. Astudillo, R. W. Allmendinger, and G. Arancibia (2014), Constructing forearc architecture over megathrust seismic cycles: Geological snapshots from the Maule earthquake region, Chile, *Geol. Soc. Am. Bull.*, 127(3–4), 464–479, doi:10.1130/B31125.1.

Arriagada, C., G. Arancibia, J. Cembrano, F. Martínez, D. Carrizo, M. Van Sint Jan, M., E. Sáez, G. González, S. Rebolledo, S. Sepúlveda, E. Contreras-Reyes, E, Jensen, and G. Yañez (2011), Nature and tectonic significance of co-seismic structures associated with the Mw 8.8 Maule earthquake, central-southern Chile forearc, *Journal of Structural Geology*, 33, 891-897, doi:10.1016/j.jsg.2011.03.004.

Astudillo, L., J. Cortés-Aranda, D. Melnick and A. Tassara (2018), Holocene deformation along the Liquiñe-Ofqui Fault Zone, southern Chile: Field observations ad geomorphic analysis, *9th Int. INQUA Meet. On Paleoseis., Act. Tectonics and Archeoseism. (PATA)*, Possidi, Greece

Barrientos, S.E. and P.S. Acevedo-Aránguiz (1992), Seismological aspects of the 1988-1989 Lonquimay (Chile) volcanic eruption. *J. Volcanol. Geotherm. Res.*, 53, 73-87, doi:10.1016/0377-0273(92)90075-O.

Barrientos, S., E. Vera, P. Alvarado, and T. Monfret (2004), Crustal seismicity in central Chile, *J. South Am. Earth Sci.*, 16, 759-768, doi:10.1016/j.jsames.2003.12.001.

Beck, M. E. (1983), On the mechanism of tectonic transport in zones of oblique subduction, *Tectonophysics,* 93(1–2), 1–11, doi:10.1016/0040-1951(83)90230-5.

Beck, M. E. (1991), Coastwise transport reconsidered: Lateral displacements in oblique subduction zones, and tectonic consequences, *Phys. Earth Planet. Inter.*, 68(1–2), 1–8, doi:10.1016/0031-9201(91)90002-Y.

Blanquat, M. D. S., B. Tikoff, C. Teyssier, and J.L. Vigneresse (1998), Transpressional kinematics and magmatic arcs, *Geological Society, London, Special Publications*, 135(1), 327–340, doi:10.1144/GSL.SP.1998.135.01.2.

Bloch, W., J. Kummerow, P. Salazar, P. Wigger, and S. Shapiro (2014), High-resolution image of the North Chilean subduction zone: seismicity, reflectivity and fluids, *Geophys. J. Int.*, 197, 1744–1749, doi:10.1093/gii/ggu084.

Bohm, M., S. Lüth, H. Echtler, G. Asch, K. Bataille, C. Bruhn, A. Rietbrock, and P. Wigger (2002), The Southern Andes between 36° and 40°S latitude: seismicity and average seismic velocities, *Tectonophysics* 356, 275–289, doi:10.1016/S0040-195(02) 00399-2.

Bommer, J., M.B. Benito, M. Ciudad-Real, A. Lemoine, M.A. López-Menjívar, R. Madariaga, Raúl, J. Mankelow, P. Méndez de Hasbun, W. Murphy, M. Nieto-Lovo, C.E. Rodríguez-Pineda and H. Rosa (2002), The El Salvador earthquakes of January and February 2001: Context, characteristics and implications for seismic risk, *Soil Dynamics and Earthquake Engineering*, 22, 389-418, 10.1016/S0267-7261(02)00024-6.

Brace, W.F. and J.D. Byerlee (1966), Stick slip as a mechanism for earthquakes, *Science*, 153(3739), 990-992.

Brasse, H., G. Kapinos, Y. Li, L. Mütschard, W. Soyer an D. Eydam (2008), Structural electrical anisotropy in the crust at the South-Central Chilean continental margin as inferred from geomagnetic transfer functions, *Phys. of the Earth and Plant. Inter.,* 173, 7-16, doi:10.1016/j.pepi.2008.10.017.

Breitkreuz, C. (1991), Permo-Carboniferous magmatism, basin development, and tectonics in the north Chilean Andes, XII International Congress on Carboniferous and Permian Geology and Stratigraphy, Abstracts, 17–18.

Byerlee, J. D., and W.F. Brace (1968), Stick slip, stable sliding, and earthquakes-Effect of rock type, pressure, strain rate, and stiffness, *J. Geophys. Res.*, 73(18), 6031–6037, doi:10.1029/JB073i018p06031.

Cardona, C., A. Tassara, L.E. Lara, C. Clifford, F. Gil and S. Morales (2015), Actividad sísmica del complejo volcánico Laguna del Maule (Chile), XIV Congreso Geológico Chileno, Actas, 222-225.

Cembrano J. and F. Hervé (1993), The Liquiñe-Ofqui Fault Zone: a major Cenozoic strike slip duplex in the Southern Andes, Second ISAG, Oxford, 21-23, 175-178.

Cembrano, J., F. Hervé and A. Lavenu (1996), The Liquine–Ofqui fault zone: a long-lived intra-arc fault system in southern Chile, *Tectonophysics,* 259, 55–66.

Cembrano, J., E. Schermer, A. Lavenu, and A. Sanhueza (2000), Contrasting nature of deformation along an intra-arc shear zone, the Liquiñe–Ofqui fault zone, southern Chilean Andes, *Tectonophysics*, 319(2), 129–149, doi:10.1016/S0040-1951(99)00321-2.

Cembrano, J., A. Lavenu, P. Reynolds, G. Arancibia, G. López and A. Sanhueza (2002), Late Cenozoic transpressional ductile deformation north of the Nazca-South America-Antarctica triple junction, *Tectonophysics*, 354, 289–314.

Cembrano, J., and L. Lara (2009), The link between volcanism and tectonics in the Southern Volcanic Zone of the Chilean Andes: A review, *Tectonophysics*, 471(1–2), 96–113, doi:10.1016/j.tecto.2009.02.038.

Chelsey, C., P. La Femina, C. Puskas and D. Kobayashi (2012), The 1707 Mw8.7 Hoei earthquake triggered the largest historical eruption of Mt. Fuji, Geophys. Res. Lett., 39(24), 1-8, doi:10.1029/2012GL053868.

Chinn, D. S., and B. L. Isacks (1983), Accurate source depths and focal mechanisms of shallow earthquakes in western South America and in the New Hebrides island arc, *Tectonics*, 2, 529–563, doi:10.1029/TC002i006p00529.

Chouet, B. (2003), Volcano Seismology, *Pure appl. geophys.*, 160, 739-788.

Cifuentes, I. (1989), The 1960 Chilean Earthquakes, *J. Geophys. Res.*, 94, B1, 665-680

Clemens, J.D. and N. Petford (1999), Granitic melt viscosity and silicic magma dynamics in contrasting tectonic settings, *J. Geol. Soc. London,* 156, 1057-1060, doi:10.1144/ gsjgs.156.6.1057.

Corti, G., E. Carminati, F. Mazzarini and M.O. Garcia (2005), Active strike-slip faulting in El Salvador, Central America, *Geology,* 33(12), 989-992, doi:10.1130/G21992.1.

Cowie, P.A. and C.H. Scholz (1992), Physical explanation for the displacemnt-length relationships of faults using a post-yield fracture mechanics model, *J. Struct. Geol.* 14, 1133-1148.

Cox, S.F. (1999), Deformational controls on the dynmcs of fluid flow in mesothermal gold systems, *Geol. Soc. London, Special Publications*, 155, 123-140, doi: 10.1144/GSL.SP.1999.155.01.10.

Cox, S.F. (2010), The application of failure mode diagrams for exploring the roles of fluid pressure and stress states in controlling styles of fracture-controlled permeability enhancement in faults and shear zones, *Geofluids*, 10, 1-2, doi: 10.1111/j.1468-8123.2010.00281.x.

De Saint Blanquat, M., B. Tikoff, C. Teyssier, and J.L. Vigneresse (1998), Transpressional kinematics and magmatic arcs, *Geol. Soc., London*, Special Publications, 135, 327-340, doi:10.1144/GSL.SP.1998.135.01.21.

Delaney, P.T., D.D.Pollard, I. Ziony and E.H. Mckee, (1986), Field relations between dikes and joints: emplacement processes and Paleostress analysis, *J. Geophys. Res.,* 91, 4920-4938.

Dzierma, Y., M. Thorwart, W. Rabbel, C. Siegmund, S. Comte, K. Bataille, P. Iglesia and C. Prezzi (2012a), Seismicity near the slip maximum of the 1960 Mw 9.5 Valdivia earthquake (Chile): Plate interface lock and reactivation of the subducted Valdivia Fracture Zone, *J. Geophy. Res.,* 117(B06312), 1-12, doi:10.1029/2011JB008914.

Dzierma, Y., W. Rabbel, M. Thorwart, I. Koulakov, H. Wehrmann, K. Hoernle and D. Comte (2012b), Seismic velocity structure of the slab and continental plate in the region of the 1960 Valdivia (Chile) slip maximum - Insights into fluid release and plate coupling, *Earth and Planetary Science Letter*s, 331-332, 164-176, doi:10.1016/j.epsl.2012.02.006.

Dziewonski, A.M., G. Ekström, J.H. Woodhouse, and G. Zwart (1990), Centroid-moment tensor solutions for January-March 1989, Phys. Earth Plan. Interiors, 59, 233-242, doi:10.1016/0031-9201(90)90232-M.

Engdahl, E., and A. Villasen˜or (2002), Global seismicity: 1900– 1999, in International Handbook of Earthquake and Engineering Seismology, Int.Geophys. Ser., vol. 81, edited by W. H. K. Lee et al., pp. 665 – 690, Academic, Amsterdam.

Farías, M., D. Comte, R. Charrier, J. Martinod, C. David, A. Tassara, F. Tapia, and A. Fock (2010), Crustal-scale structural architecture in central Chile based on seismicity and surface geology: Implications for Andean mountain building, Tectonics, 29, TC3006, doi:10.1029/ 2009TC002480.

Farías, M., D. Comte, S. Roecker, D. Carrizo, and M. Pardo (2011), Crustal extensional faulting triggered by the 2010 Chilean earthquake: The Pichilemu seismic sequence, *Tectonics*, 30, TC6010, doi:10.1029/2011TC002888.

Fitch, T. J. (1972), Plate Convergence, Transcurrent Faults, and Internal Deformation Adjacent to Southeast Asia and the Western Pacific, *J. Geophy. Res.*, 77(23), 4432–4460.

Foulger, G.R. and R.E. Long (), Non-double couple earthquake focal mechanism, in: Gasparini, P., R. Scarpa, and K. Aki (Eds.), Volcanic Seismology, Springer-Verlag, doi:10.1007/978-3-642-77008-1.

Glodny, J., H. Echtler, S. Collao, M. Ardiles, P. Buron, and O. Figueroa (2008), Differential Late Paleozoic active margin evolution in South-Central Chile (37°S–40°S)—The Lanalhue Fault Zone, *J. South Am.*

Earth Sci., 26(4), 397–411, doi:10.1016/j.jsames.2008.06.001.

Gratier, J.P. (2011), Fault Permeability and Strength Evolution Related to Fracturing and Healing Episodic Processes (Years to Millennia): the Role of Pressure Solution, *OGST - Revue d'IFP Energies nouvelles,* 66, 491-506, doi:10.2516/ogst/2010014.

Griffn, W.L. and S.Y. O'Reilly (1987), Is the continental Moho the crust-mantle boundary? *Geology*, 15,241-244, doi:10.1130/0091-7613(1987)15<241:ITCMTC>2.0.CO;2

Gudmundsson, A. (2011), Rock Fractures in Geological Processes, Cambridge University Press, ISBN:978-0-521-86392-6.

Haberland, C., A. Rietbrock, D. Lange, K. Bataille and S. Hofmann (2006), Interaction between continental forearc and oceanic plate at the South-Central Chilean margin as seen in local earthquake data, *Geophys. Res. Lett.*, 33, L23302, doi:10.1029/2006GL028189.

Haberland, Ch, A. Rietbrock, D. Lange, K. Bataille and T. Dahm (2009), Structure of the seismogenic zone of the southcentral Chilean margin revealed by local earthquake traveltime tomography, *J. geophys. Res.*, 114, B01317, doi:10.1029/2008JB005802.

Hauser, A. (1997), Catastro y Caracterización de las Fuentes de Aguas Minerales y Termales de Chile, *Servicio Nacional de Geología y Minería*, Boletín 50, (In Spanish).

Hill, D. (1977), A model for earthquake swarms, *J. Geophys. Res.*, 82(8), 1347-1352.

Husen, S., E. Kissling, E. Flüh, and G. Ash (1999), Accurate hypocenter determination in the seismogenic zone of the subducting Nazca plate in north Chile using a combined on-/offshore network, *Geophys. J. Int.*, 138, 687–701.

Iturrieta, P., D. Hurtado, J. Cembrano and A. Stanton-Yonge (2017), States of stress and slip partitioning in a continental scale strike-slip duplex: Tectonic and magmatic implications by means of finite element modeling, *Earth and Planetary Science Letter*s, 473, 71-82, doi: 10.1016/j.epsl.2017.05.041.

Jarrard, R. D. (1986), Terrane motion by strike-slip faulting of forearc slivers. *Geology*, 14(9), 780–783.

Jay, J. A., M.E. Pritchard, M. E. West, D. Christensen, M. Haney, E. Minaya and M. Zabala (2011), Shallow seismicity, triggered seismicity , and ambient noise tomography at the long-dormant Uturuncu Volcano, Bolivia, *Bull. Volcanol.* 74 (4), 817–837, doi:10.1007/s00445-011-0568-7

Joussineau, G. and A. Aydin (2009), Segmentation along Strike-Slip Faults Revisited, *Pure app. geophys.* 166, 1575-1594, doi: 10.1007/s00024-009-0511-4.

Kaizuka, S. (1968), A tectonic model for the morphology of arc-trench systems, especially for the echelon ridges and mid-arc faults, *Jpn. J. Geol. Geogr.*, 45, 9-28

Kanamori, H. and G.S. Stewart (1979), A slow earthquake, *Phys. Earth Planet. Inter.*, 18, 167-175

Katz, H. R. (1971), Continental margin in Chile; is tectonic style compressional or extensional?, Am. Assoc. Pet. Geol. Bull., 55(10), 1753–1758.

Kim, Y-S., D. Peacock D.C.P. and D.J. Sanderson (2002), Fault damage zones, *J. Sruct. Geol.*, 26, 503-517, doi: 10.1016/j.jsg.2003.08.002

Kimura, G. (1986), Oblique subduction and collision: Forearc tectonics of the Kuril arc, Geology, 14, 404-407.

Kissling, E., (1988), Geotomography with local earthquakes, Rev. Geophys., 26, 659–698.

Kissling, E., W.L. Ellsworth, D. Eberhart-Phillips, and U. Kradolfer (1994), Initial reference models in local earthquake tomography, *J. Geophys. Res.*, 99, 19635–19646.

Kissling, E., U. Kradolfer, and H. Maurer (1995), VELEST User's Guide: Short Introduction, Institute of Geophysics and Swiss Seismological Service, ETH, Zurich.

Kisslinger, C., (1980), Evaluation of S to P amplitude ratios for determining focal mechanisms from regional network observations, *Bull. seism. Soc. Am.*, 70, 999–1014.

Koulakov, I., S. Sobolev, and G. Asch (2006), P- and S- velocity images of the lithosphere-asthenosphere system in the central Andes from local-source tomographic inversion, *Geophys. J. Int.*, 167, 106–126.

La Femina, P. C., T.H. Dixon and W. Strauch (2002), Bookshelf faulting in Nicaragua, *Geology,* 30(8), 751–754.

Lange, D., A. Rietbrock, C. Haberland, K. Bataille, T. Dahm, F. Tilmann, and E. Flüh (2007), Seismicity and geometry of the south Chilean subduction zone (41.5°S–43.5°S): implications for controlling parameters, *Geophys. Res. Lett.*, 34, L06311, doi:10.1029/2006GL029190.

Lange, D., J. Cembrano, A. Rietbrock, C. Haberland, T. Dahm and K. Bataille (2008), First seismic record for intra-arc strike-slip tectonics along the Liquiñe-Ofqui fault zone at the obliquely convergent plate margin of the Southern Andes, *Tectonophysics*, 455, 14–24, doi:10.1016/j.tecto.2008.04.014.

Lange, D., F. Tilmann, S. Barrientos, E. Contreras-Reyes, P. Methe, M. Moreno, B. Heit, H. Agurto, B. Pascal, J.P. Vilotte, and S. Beck (2012), Aftershock seismicity of the 27 February 2010 Mw 8.8 Maule earthquake, Earth and Plan. Sci. Lett., 317, 412-425, doi:10.1016/j.epsl.2011.11.034.

Lara, L. E., J. Cembrano, and A. Lavenu (2008), Quaternary vertical displacement along the Liquiñe-Ofqui fault zone: Differential Uplift and coeval volcanism in the Southern Andes?, *Int. Geol. Rev.*, 50, 975–993, doi:10.2747/0020-6814.50.11.975.

Lavenu, A., and J. Cembrano (1999), Compressional and transpressional stress pattern for the Pliocene and Quaternary (Andes of central and southern Chile), *J. Struct. Geol.*, 21, 1669–1691, doi:10.1016/S0191-8141(99)00111-X.

Legrand, D., S. Barrientos, K. Bataille, J. Cembrano and A. Pavez (2010), The fluid-driven tectonic swarm of Aysen Fjord, Chile (2007) associated with two earthquakes (Mw = 6.1 and Mw = 6.2) within the Liquiñe Ofqui Fault Zone, *Cont. Shelf Res.*, 31, 151–154, doi:10.1016/j.csr.2010.05.008.

Lira, E., G. Sielfeld, A. Bosch, R. Castellón, D. Cumming, R. Figueroa, I. Gottreux, A. Gutierrez, P. Iturrieta, J. Maringue, J.J. Muñoz, N. Pérez, I. Santibañez and G. Yañez (2015), Reactivación de fallas de larga vida trasversales al orógeno andino. Persectivas desde la Falla Pichilemu, XIV Congreso Geológico Chileno.

Lienert, B. R. E., E. Berg, and L.N. Frazer (1986), Hypocenter: An earthquake location method using centered, scaled, and adaptively least squares, *Bull. Seismol. Soc. Am.*, 76, 771–783.

Lienert, B. R. E. and J. Havskov (1995), A computer program for locating earthquakes both locally and globally, *Seis. Res. Lett.*, 66, 26–36.

Lomax, A., J. Virieux, P. Volant and C. Berge (2000), Probabilistic earthquake location in 3D and layered models: Introduction of a Metropolis-Gibbs method and comparison with linear locations, in Thurber, C.H., and N. Rabinowitz (eds.), Advances in Seismic Event Location Kluwer, Amsterdam, 101-134.

Manga, M., and E. Brodsky (2006), Seismic Triggering of Eruptions in the Far Field: Volcanoes and Geysers, *Annu. Rev. Earth Planet. Sci.*, 34, 263-291, doi:10.1146/annurev.earth.34.031405.125125.

McCaffrey, R. (1992), Oblique plate convergence, slip vectors, and forearc deformation, *J. Geophys. Res.*, 97(B6), 8905-8915, doi:10.1029/92JB00483.

McCaffrey, R. (1996), Estimates of modern arc-parallel strain rates in fore arcs, *Geology,* 24(1), 27-30.

McCloskey, J., S.S. Nalbamt, S. Steacy (2005), Earthquake risk from co-seismic stress, Nature, 434, doi: 10.1038/434291a.

Melnick, D., A. Folguera and V.A. Ramos (2006a), Structural control on arc volcanism: the Caviahue-Copahue complex, Central to Patagonian Andes transition (38˚S). *J. South Am. Earth Sci.,* 22, 66-88, doi:10.1016/j.jsames.2006.08.008.

Melnick, D., M. Rosenau, A. Folguera, and H.Echtler (2006b), Neogene tectonic evolution of the Neuquén Andes western flank (37–39°S), Special Paper in Kay, S.M, and V.A. Ramos, Evolution of an Andean Margin: A Tectonic and Magmatic View from the Andes to the Neuquén Basin (35°-39°S lat), *Geological Society of America*, 407, 73–95, doi: 10.1130/2006.2407(04)

Melnick, D., and H. P. Echtler (2006), Morphotectonic and geologic digital map compilations of the South-Central Andes (36°–42°S), in *The Andes-Active Subduction Orogeny: Frontiers in Earth Sciences*, edited by O. Oncken et al., pp. 565–568, Springer, Berlin.

Melnick, D., B. Bookhagen, M. R. Strecker, and H. P. Echtler (2009), Segmentation of megathrust rupture zones from fore-arc deformation patterns over hundreds to millions of years, Arauco peninsula, Chile, J. Geophys. Res., 114, B01407, doi:10.1029/2008JB005788.

Mitchell, T.M. and Faulkner D.R. (2009), The nature and origin of off-fault damage sorrounding strike-slip fault zones with a wide range of displacements: A field study from the Atacama fault system, northern Chile, *J. Struct. Geol.* 31, 802-816, doi: 10.1016/j.jsg.2009.05.002.

Mora-Stock C., D. Comte, R. Russo, A. Gallego, and V. Mocanu (2010), Aysén seismic swarm (January 2007) in southern Chile: analysis using joint hypocentral determination. *J. Seismol.,* 14 (4), 683-691, doi:10.1007/s10950-010-9190-y.

Mora-Stock, C., M. Thorwart, T. Wunderlich, S. Bredemeyer, T.H. Hansteen, and W. Rabbel (2012), Comparison of seismic activity for Llaima and Villarrica volcanoes prior to and after the Maule 2010 earthquake, *Int. J. Earth Sci*. 103(7), 2015–2028. doi:10.1007/s00531-012-0840-x.

Moreno, M.S., J. Klotz, D. Melnick, H. Echtler and K. Bataille (2008), Active faulting and heterogeneous deformation across a megathrust segment boundary from GPS data, south central Chile (36 − 39°S), *Geochem. Geophys. Geosyst.*, 9, Q12024, doi:10.1029/2008GC002198.

Moreno, M.S., J. Bolte, J. Klotz, D. Melnick (2009), Impact of megathrust geometry on inversion of coseismic slip from geodetic data: application to the 1960 Chile earthquake, *Geophys. Res. Lett.* 36, doi:10.1029/2009GL039276.

Moreno, M.S, D. Melnick, M. Rosenau, J. Bolte, J. Klotz, H. Echtler, J. Baez, K. Bataille, J. Chen, M. Bevis, H. Hase, O. Oncken (2011), Heterogeneous plate locking in the South-Central Chile subduction zone: Building up the next great earthquake, *Earth Planet. Sci. Lett.*, 305(3–4), 413–424, doi:10.1016/j.epsl.2011.03.025.

Moreno, M.S., et al. (2012), Toward understanding tectonic control on the Mw 8.8 2010 Maule Chile earthquake, *Earth Planet. Sci. Lett.*, 321–322, 152–165, doi:10.1016/j.epsl.2012.01.006.

Mori, J., R.A. White, D. H. Harlow, P. Okubo, J.A. Power, R.P. Hoblitt, E.P. Laguerta, A. Lanuza and B.C. Bautista (1991), Volcanic Earthquakes following the 1991 Climatic Eruption of Mount Pinatubo: Strong Seismicity during a Waning Eruption, *U.S. Geological Survay Publocations,*

https://pubs.usgs.gov/pinatubo/mori1/.

Moser, T.J., T. van Eck and G. Nolet (1992), Hypocenter determination in strongly heterogeneous earth models using the shortest path method, *J. Geophys. Res.*, 97, 6563-6572.

Nacif, S., M. Lupari, E.G. Triep, A. Nacif, O. Álvarez, A. Folguera, M. Gímenez (2017), Change in the pattern of crustal seismicity at the Southern Central Ande from local seismic network, *Tectonophysics*, 708, 56-69, doi: 10.1016/j.tecto.2017.04.012

Nakamura, K. (1977), Volcanoes as possible indicators of tectonic stress orientation e principle and Proposal, *J. Volc. and Geoth. Res.*, 2, 1-16, doi:10.1007/BF01637099.

Naranjo, J.A. (2015), Nuevo estilo eruptivo del volcán Villarrica: 3 de marzo 2015, Actas XiV Congreso Geológico Chileno.

Observatorio Volcanologico de los Andes del Sur -OVDAS-, (2015), Volcanic activity reports (RAV, Reportes de Actividad Volcánica), 1 -13.

Ottemöller, L. and J. Havskov (2003), Moment magnitude determination for local and regional earth- quakes based on source spectra, *Bull. Seismol. Soc. Am.*, 93, 203–214.

Ottemöller L., P. Voss and J. Havskov (2014), Seisan earthquake analysis software for Windows, Solaris, Linux and Macosx, http://seisan.info.

Pankhurst, R.J., C.W. Rapela, C.M. Fanning and M. Márquez (2006), Gondwanide continental collision and the origin of Patagonia, *Earth Sci. Rev.,* 76, 235-257, doi:10.1016/j.earscirev.2006.02.001.

Pardo-Casas, F., and P. Molnar (1987), Relative motion of the Nazca (Farallón) and South American plates since late Cretaceous times, *Tectonics,* 6, 233–248, doi:10.1029/TC006i003p00233.

Patanè, D., M. Aliotta, A. Cannata, C. Cassisi, M. Coltelli, G. Di Grazia, P. Montalto and L. Zuccarello (2011), Interplay between Tectonics and Mount Etna's Volcanism: Insights into the Geometry of the Plumbing System, New Frontiers in Tectonic Research - At the Midst of Plate Convergence, Dr. Uri Schattner (Ed.), *InTech,* doi: 10.5772/23503.

Pérez-Flores, P., J. Cembrano, P. Sánchez-Alfaro, E. Veloso, G. Arancibia and T. Roquer, (2016), Tectonics, magmatism and paleo-fluid distribution in a strike-slip setting: in- sights from the northern termination of the Liquiñe-Ofqui fault system, Chile. *Tectonophysics,* 680, 192–210, doi: 10.1016/j.tecto.2016.05.016.

Pérez-Flores, P., E. Veloso, J. Cembrano, P. Sánchez-Alfaro, M. Lizama and G. Arancibia (2017), Fracture network, fluid pathways and paleostress at the Tolhuaca gethermal field, *J. Struc. Geol.*, 96, 134-148, doi:10.1016/j.jsg.2017.01.009.

Potent, S. (2003), Kinematik und Dynamik neogener Deformationsprozesse des südzentralchilenischen Subduktionssystems, nördlichste Patagonische Anden (37 -40˚S), Ph.D thesis, University of Hamburg.

Polloitz, F.F., P. Banerjee, R. Bürgmann, M. Hashimoto and N. Choosakul (2006), Stess changes along the Sunda trench following the 26 December 2004 Sumatra-Adaman and 28 March 2005 Nias earthquakes, *Geophy. Res. Lett.,* 33, L06309, doi: 10.1029/2005GL02558.

Rapela, C.W., R.J. Pankhurst, C.M. Fanning and L.E. Grecco (2003), Basement evolution of the Sierra de la Ventana Fold Belt: new evidence for Cambrian continental rifting along the southern margin of Gondwana, *Journal of the Geological Society, London* 160, 613–628.

Reasenberg, P. and D. Oppenheimer (1985), Fpfit, fpplot, and fppage: Fortran computer programs for calculating and displaying earthquake fault plane solutions,Technical report, U.S. Geol. Survey.

Reid, H.F. (1913), Sudden earth-movements in Sumatra in 1892, *Bulletin of the Seismological Society of America,* 3, 72–79.

Risacher, F. and A. Hauser (2008), Catastro de las proncipales fuentes de aguas termanles de Chile, *Servicio Nacional de Geología y Minería y Institut de Recherche pour le Déceloppement (IRD-France)*, Santiago, 1-81.

Rivera, O.M. and J. Cembrano (2000), Modelo de formación de cuencas volcano-tectónicas en zonas de transferencia oblicuas a la cadena Andina: el caso de las cuencas Oligo-Miocenas de Chile central y su relación con estructuras WNW-NW (33-34˚30'), IX Congreso Geológico Chileno, II, 649-654.

Roquer, T., G. Arancibia, J. Rowland, P. Iturrieta, D. Morata and J. Cembrano (2017), Fault-controlled development of shallow hydrothermal systems: structural and mineralogical insights from the Southern Andes. *Geothermics* 66, 156–173. doi:10.1016/j.geothermics.2016.12.003.

Roman, D.C. (2005), Numerical models of volcano-tectonic earthquake triggering on non-ideally oriented faults, *Geophys. Res. Lett.*, 32, L02304, doi:10.1007/s00445-002-0201x.

Roman, D.C. and K.V. Cashman (2006), The origin of volcano-tectonic earthquake swarms, Geology, 34(6),457-460, doi:10.1130/G22269.1.

Rosenau, M., D. Melnick, and H. Echtler (2006), Kinematic constraints on intra-arc shear and strain partitioning in the southern Andes between 38°S and 42°S latitude, *Tectonics*, 25, TC4013, doi:10.1029/2005TC001943.

Rowland, J.V. and R.H. Sibson (2004), Structural controls on hydrothermal flow in a segmented rift system, Taupo Volcanic Zone, New Zealand, *Geofluids,* 4, 259-283.

Salazar P., J. Kummerow, P. Wigger, S. Shapiro, and G. Asch (2017), State of stress and crustal fluid migration related to west-dipping structures in the slab-forearc system in northern Chilean subduction zone, *Geophys. J. Int.*, 208, 1403-1413, doi:10.1093/gii/ggw463.

Sánchez, L., and H. Drewes (2016), Crustal deformation and surface kinematics after the 2010 earthquakes in Latin America, J. of Geodynamics, 1442, doi: 10.1016/j.jog.2016.06.05.

Sánchez-Alfaro, P., P. Pérez-Flores, G. Arancibia, J. Cembrano, and M. Reich (2013), Crustal deformation effects on the chemical evolution of geothermal systems: The intra-arc Liquiñe–Ofqui fault system, Southern Andes, *Int. Geol. Rev.*, 55(11), 1384–1400, doi:10.1080/00206814.2013.775731.

Savage, H. M. and E. Brodsky (2011), Collateral damage: Evolution with displacement of fracture distribution and secondary fault strands in fault damag zones, *J. Geophy. Res.*, 116, doi: 10.1029/2010JB007665.

Scholz, C.H. (1987), Wear and gouge formation in brittle faulting, *Geology*, 15, 493-495.

Scholz, C.H. (1988), The brittle-plastic transition and the depth of seismic faulting, *Geologische Rundschau,* Stuttgart, 77, 319-328.

Scholz, C. H. (1998), Earthquakes and friction laws, *Nature*, 391, 37–42. doi:10.1038/34097.

Scholz, C. H. (2002), The Mechanics of Earthquakes and Faulting (2nd Edition), *Cambridge Uni. Press.*

Sernageomin - Servicio Nacional de Geología y Minería - (2002), Mapa geológico de Chile, scale 1:1,000,000, *Map M61*, Santiago, Chile.

Sibson, R.H., J. Moore and H. Rankin (1975), Seismic pumping - a hydrothermal fluid transport mechanism, *J. Geol. Soc. Lond.*, 131, 653-659, doi: 10.1144/gsjgs.131.6.0653

Sibson, R. (1984), Roughness at the Base of the Seismogenic Zone: Contributing Factors, *J. Geophys. Res.*, 89, 5791-5799.

Sibson, R. (2002), Geology of the Crustal Earthquake Source. In Lee, W.H.K.; Kanamori, H.; Jennings, P.; Kisslinger, C. (eds.), International Handbook of Earthquake and Engineering Seismology, *Academic Press*, 81A (29), 455-473.

Siebert, L., T. Simkin, and P. Kimberly (2010), Volcanoes of the World (3rd Ed.), Smithsonian Institution, University of California Press, ISBN: 978-0-520-26877-7.

Sieh K. and D. Natawidjaja (2000), Neotectonics of the Sumatran fault, Indonesia, *J. Geophy. Res.*, 105(B12), 28295-28326.

Sielfeld, G., J. Cembrano, and L. Lara (2017), Transtension driving volcano-edifice anatomy: Insights from Andean transverse-to-the-orogen tectonic domains, *Quat. Int.*, 438, 22-39, doi:10.1016/j.quaint.2016.01.002.

Snoke, J. A., J.W. Munsey, A.G. Teague, and G.A. Bollinger (1984), A program for focal mechanism determination by combined use of polarity and SV-P amplitude ratio data, *Earthquake note*s, 55.

Springer, M. (1999), Interpretation of heat-flow density in the Central Andes, *Tectonophysics*, 306, 377–395.

Stanton-Yonge, A., W.A. Griffith, J. Cembrano, R.St. Julien and P. Iturrieta (2016), Tectonic role of margin-parallel and margin-transverse faults during oblique subduction in the southern volcanic zone of the Andes: insights from boundary element modeling, *Tectonics,* 35, 1990–2013, doi:10.1002/ 2016TC004226.

Stesky, R.M. (1975), The mechanical behavior of faulted rock at high temperature and pressure, Ph.D thesis, Massachusetts Institute of Technology.

Suzuki, Y., S. Ioka and H. Muraoka (2014), Determining the maximum depth of hydrothermal circulation using geothermal mapping and seismicity to delineate the depth to brittle-plastic transition in northern Honshu, Japan, *Energies*, 7, 3503-3511, doi:10.3390/en7053503.

Tankard, A.J., M. A. Uliana, H. J. Welsink, V. A. Ramos, M. Turic, A. B. França, E. J. Milani, B. B. de Brito Neves, N. Eyles, J. Skarmeta, H. Santa Ana, F. Wiens, M. Cirbián, O. López-Paulsen, G.J.B. Germs, M.J. de Wit, T. Machacha, R.McG. Miller (1995), Tectonic controls of basin evolution in southwestern Gondwana, in Tankard A. J., R. Suárez S., and H. J. Welsink, *Petroleum basins of South America: AAPG,* 62, 5–52.

Tardani, D., M. Reich, E. Roulleau, N. Takahata, Y. Sano, P.Pérez-Flores, P. Sánchez-Alfaro, J. Cembrano, G. Arancibia (2016), Exploring the structural controls on helium, nitrogen and carbon isotope signatures in hydrothermal fluids along an intra- arc fault system, *Geochim. Cosmochim.* 184, 193-211, doi: 10.1016/j.gca.2016.04.031.

Tarantola, A. and B. Valette (1982), Inverse problems = quest for information, *J. Geophys.*, 50, 159-170.

Tarantola, A. (1987), Inverse problem theory: Methods for data fitting and model parameter estimation, Elsevier, Amsterdam, 613.

Tikoff, B., and C. Teyssier (1994), Strain modeling of displacement-field partitioning in transpressional orogens, Journal of Structural Geology, 16(11), 1575–1588, doi:10.1016/0191-8141(94)90034-5.

Tikoff B., and M. de Saint Blanquat (1997), Transpressional shearing and strike-slip partitioning in the Late Cretaceous Sierra Nevada magmatic arc, California, Tectonics, 16(3), 442-459.

Turcotte, D.L. (1997), Fractals and Chaos in Geology and Geophysics, 2nd ed. Cambridge University Press,

Cambridge.

Utsu, T. (2002), Statistical Features of Seismicity, in Lee, W., H. Kanamori, P.C. Jennings and C. Kisslinger (eds.), International Handbook of Earthquake & Engineering Seismology, Part A, 719-732.

Wang, K., Y. Hu, M. Bevis, E. Kendrick, R. Smalley, R. B. Vargas, and E. Lauría (2007), Crustal motion in the zone of the 1960 Chile earthquake: Detangling earthquake-cycle deformation and forearc-sliver translation, *Geochem. Geophys. Geosyst*., 8, Q10010, doi:10.1029/ 2007GC001721.

Weller, O., D. Lange, F. Tilmann, D. Natawidjaja, A. Rietbrock, R. Collings and L. Gregory (2012), The structure of the Sumatran Fault revealed by locacl seismicity, *Geophy. Res. Lett.,* 39, 1-7, doi: 10.1029/2011GL050440.

White, R.A. (1991), Tectonic implications of upper-crustal seismicity in Central America, in *Neotectonics of North America*: Slemmons, D.B., E.R. Engdahl, M.D. Zoback and D. Blackwell (Editors), Boulder Colorado, *Geol. Soc. Am*., pp. 323-338.

White, R. A, and D.H. Harlow (1993), Destructive upper-crustal earthquakes of Central America since 1900, *Bull. of the Seis. Soc. of Am.,* 83(4), 1115–1142.

Wigger, P. et al., 1994. Variation of the crustal structure of the Southern Central Andes deduced from seismic refraction investigations, in Reutter, K.-J., E. Scheuber, and P. Wigger (eds.), Tectonics of the Sourthern Central Andes, 23–48, ed. Springer Verlag, doi:10.1007/978-3-642-77353-2_2.

Wittlinger, G., G. Herquel, and T. Nakache (1993), Earthquake location in strongly heterogeneous media, *Geophys. J. Int.*, 115, 759-777.

Wrage, J., D. Tardani, M. Reich, L. Daniele, G. Arancibia, J. Cembrano, P. Sánchez-Alfaro, D. Morata, R. Pérez-Moreno (2017), Geochemistry of thermal waters in the Southern Volcanic Zone, Chile - Implications for structural controls on geothermal fluid composition, Chemical Geology, 466, 545-561, doi:10.1016/j.chemgeo.2017.07.004.

Yamaguchi, A., S.F. Cox, G. Kimura and S. Okamoto (2011), Dynamic changes in fluid redox state associated with episodic fault rupture along a megasplay fault in a subduction zone, Earth and Planetary Science Letters, 302, 369-377, doi: 10.1016/j.epsl.2010.12.029.

Yáñez, G., P. Gana, and R. Fernández (1998), Origen y significado geológico de la Anomalía Melipilla, Chile Central, *Revista Geológica de Chile*, 25, 175-198.

Yáñez, G., and J. Cembrano (2004), Role of viscous plate coupling in the late Tertiary Andean tectonics, *J. Geophys. Res*., 109, B02407, doi:10.1029/ 2003JB002494.

Yoon, M., S. Buske, R. Schulze, S. Lueth, S. Shapiro, M. Stiller, and P. Wigger (2003), Along strike variations of crustal reflectivity related to the Andean subduction process, *Geophys. Res. Lett*., 30, doi:10.1029/2002GL015848.

Yoon, M., S. Buske, S.A.Shapiro, and P. Wigger (2009), Reflection Image Spectroscopy across the Andean subduction zone, *Tectonophysics*, 472, 51–61, doi:10.1016/j.tecto.2008.03.014.

Yuan, X., S.V. Sobolev, R. Kind, O. Oncken, and Andes Seismology Group (2000), New constraints on subduction and collision processes in the central Andes from P-to-S converted seismic phases, Nature, 408, 958–961.

Yuan, X., G. Asch, K. Bataille, G. Bock, M. Bohm, H. Echtler, R. Kind, O. Oncken, and I. Wölbern (2006), Deep seismic images of the Southern Andes, in Kay, S.M., and V.A. Ramos (eds.), Evolution of an Andean margin: A tectonic and magmatic view from the Andes to the Neuquén Basin (35˚-39˚S lat), *J. Geol. Soc. Am*, Special Paper 407, 61-72, doi:10.1130/2006.2407(03).

Zobin, V.M. (2003), Introduction to volcanic seismology, Elsevier Science B.V., ISBN:0-444-51340-X.